

**IRAK1-dependent Regnase-1-14-3-3 complex formation controls Regnase-1-mediated  
mRNA decay**

Kotaro Akaki<sup>1,2</sup>, Kosuke Ogata<sup>3</sup>, Yuhei Yamauchi<sup>4</sup>, Noriki Iwai<sup>1</sup>, Ka Man Tse<sup>1</sup>, Fabian Hia<sup>1</sup>,  
Atsushi Mochizuki<sup>4</sup>, Yasushi Ishihama<sup>3</sup>, Takashi Mino<sup>1</sup>, and Osamu Takeuchi<sup>1\*</sup>

<sup>1</sup>Department of Medical Chemistry, Graduate School of Medicine, Kyoto University, Kyoto  
606-8501, Japan

<sup>2</sup>Graduate School of Biostudies, Kyoto University, Kyoto 606-8501, Japan

<sup>3</sup>Department of Molecular and Cellular BioAnalysis, Graduate School of Pharmaceutical  
Sciences, Kyoto University, Kyoto 606-8501, Japan

<sup>4</sup>Laboratory of Mathematical Biology, Institute for Frontier Life and Medical Sciences,  
Kyoto University, Kyoto 606-8507, Japan

\*Correspondence: [otake@mfour.med.kyoto-u.ac.jp](mailto:otake@mfour.med.kyoto-u.ac.jp) (O.T.)

**Abstract**

Regnase-1 is an endoribonuclease crucial for controlling inflammation by degrading mRNAs encoding cytokines and inflammatory mediators in mammals. However, it is unclear how Regnase-1-mediated mRNA decay is controlled in interleukin (IL)-1 $\beta$ - or Toll-like receptor (TLR) ligand-stimulated cells. Here, by analyzing the Regnase-1 interactome, we found that IL-1 $\beta$  or TLR stimulus dynamically induced the formation of Regnase-1- $\beta$ -transducin repeat-containing protein ( $\beta$ TRCP) complex. Importantly, we also uncovered a novel interaction between Regnase-1 and 14-3-3 in both mouse and human cells. In IL-1R/TLR-stimulated cells, the Regnase-1-14-3-3 interaction is mediated by IRAK1 through a previously uncharacterized C-terminal structural domain. Phosphorylation of Regnase-1 at S494 and S513 is critical for Regnase-1-14-3-3 interaction, while a different set of phosphorylation sites of Regnase-1 is known to be required for the recognition by  $\beta$ TRCP and proteasome-mediated degradation. We found that Regnase-1-14-3-3 and Regnase-1- $\beta$ TRCP interactions are not sequential events. Rather, 14-3-3 protects Regnase-1 from  $\beta$ TRCP-mediated degradation. On the other hand, 14-3-3 abolishes Regnase-1-mediated mRNA decay by inhibiting Regnase-1-mRNA association. In addition, nuclear-cytoplasmic shuttling of Regnase-1 is abrogated by 14-3-3 interaction. Taken together, the results suggest that a novel inflammation-induced interaction of 14-3-3 with Regnase-1 stabilizes inflammatory mRNAs by sequestering Regnase-1 in the cytoplasm to prevent mRNA recognition.

## Introduction

The expression of proinflammatory cytokines is the hallmark of innate immune responses against microbial infection. Whereas inflammatory responses are critical for the elimination of invading pathogens, excess and chronic inflammation can culminate in tissue destruction and autoimmune diseases. When innate immune cells encounter pathogen-associated molecular patterns (PAMPs) or damage-associated molecular patterns (DAMPs), they are sensed by pattern-recognition receptors such as Toll-like receptors (TLRs), triggering the transcription of inflammatory genes (Fitzgerald & Kagan, 2020; Takeuchi & Akira, 2010).

The expression of inflammatory genes is also controlled by post-transcriptional mechanisms to facilitate or limit inflammatory responses (Anderson, 2010; Carpenter et al., 2014; Turner & Díaz-Muñoz, 2018). Regnase-1 (also referred to as Mcpip1, Gene name: *Zc3h12a*), an RNase, is a critical regulator of inflammation. Regnase-1 binds to and degrades inflammatory mRNAs such as *Il6* or *Il12b* by recognizing stem-loop structures present in the 3' untranslated regions (Matsushita et al., 2009; Mino et al., 2015). *Zc3h12a*-deficient mice exhibit an autoimmune phenotype, indicating its importance as a negative regulator of inflammation (Matsushita et al., 2009; Uehata et al., 2013). Regnase-1 efficiently suppresses the expression of its target genes by degrading CBP80-bound mRNAs during the pioneer-round of translation by associating with ribosome and a helicase protein, UPF1 (Mino et al., 2015, 2019). CBP80 binds to newly synthesized mRNAs in the nucleus and is replaced by eIF4E after the pioneer round of translation following mRNA export from the nucleus (Maquat et al., 2010; Müller-Mcnicoll & Neugebauer, 2013). Thus, it is possible that

Regnase-1 recognizes target mRNAs in the steps leading to the pioneer round of translation.

The stability of cytokine mRNAs is dynamically regulated in innate immune cells under inflammatory conditions (Carpenter et al., 2014; Hao & Baltimore, 2009; Turner & DÍaz-Muñoz, 2018). Post-translational control of Regnase-1 in response to inflammatory stimuli contributes to extending half-lives of inflammatory mRNAs. Stimulation of cells with TLR-ligands, IL-1 $\beta$ , or IL-17 results in the activation of I $\kappa$ B kinases (IKKs), which phosphorylate Regnase-1 at S435 and S439, in addition to I $\kappa$ B $\alpha$  (Iwasaki et al., 2011; Kakiuchi et al., 2020; Nanki et al., 2020; Tanaka et al., 2019). Regnase-1, phosphorylated at S435 and S439 is subsequently recognized by  $\beta$ TRCP, one of the components in the SKP1-CUL1-F-box (SCF) complex, which induces K48-linked polyubiquitination of Regnase-1, followed by proteasome-mediated degradation (Iwasaki et al., 2011). On the other hand, these stimuli also induce transcription of *Zc3h12a* (Iwasaki et al., 2011). Consequently, the protein level of Regnase-1 drastically changes during these stimulations; Regnase-1 levels decrease immediately after the stimulation and then increase to levels higher than its pre-stimulation. However, the post-translational regulatory mechanism of Regnase-1 following inflammatory stimuli is still not fully elucidated.

14-3-3 family proteins are conserved among species and are known to form hetero- or homo-dimer (Aitken, 2006; Pennington et al., 2018). The 14-3-3 dimer binds to various phosphorylated proteins using its two phosphor-S/T binding pockets which recognize unique phospho-peptides (Muslin et al., 1996; Yaffe et al., 1997). Although 14-3-3 itself has no enzymatic activity, 14-3-3 is known to modulate the properties of target proteins, such as



80 protein stability or localization (Aitken, 2006; Pennington et al., 2018).

81         In this study, we utilized an interactome-based approach to isolate Regnase-1 protein  
82 complexes and found that TLR-ligand, IL-1 $\beta$ , or IL-17 stimulation induces the formation of  
83 the Regnase-1-14-3-3 complex. The phosphorylation of Regnase-1 at S494 and S513 is  
84 responsible for binding with 14-3-3, which in turn stabilizes Regnase-1 protein by excluding  
85  $\beta$ TRCP. However, 14-3-3-bound Regnase-1 is not functional because 14-3-3 prevents  
86 Regnase-1 from recognizing target mRNAs. In addition, we found that nuclear-cytoplasmic  
87 shuttling of Regnase-1 is inhibited by 14-3-3's association with Regnase-1. Collectively, we  
88 identified a novel 14-3-3-mediated molecular mechanism which controls Regnase-1; a  
89 distinctly independent mechanism from  $\beta$ TRCP-mediated protein degradation of Regnase-1.

90

## Results

### Regnase-1 interactome analysis revealed dynamic recruitment of 14-3-3 upon stimulation

To comprehensively uncover Regnase-1-associating proteins in steady state and under inflammatory conditions, we stimulated HeLa cells expressing FLAG-HA-tagged Regnase-1 with or without IL-1 $\beta$  and immunoprecipitated Regnase-1 immediately after the treatment with a crosslinking reagent, Dithiobis(succinimidyl propionate) (DSP) (Figure 1A). Consistent with the previous reports, mass spectrometry analysis revealed that Regnase-1 interacted with translation-related proteins such as ribosomal proteins in unstimulated cells (Mino et al., 2015). Whereas IL-1 $\beta$  stimulation reduced the association between Regnase-1 and translation-related proteins, the stimulation strongly induced the association between Regnase-1 and SCF complex proteins such as  $\beta$ TRCP1/2, CUL1, and SKP1 (Iwasaki et al., 2011). In addition to these proteins, we identified 14-3-3 family proteins as novel Regnase-1-associating proteins under IL-1 $\beta$ -stimulated conditions (Figure 1B). Consistently, immunoprecipitation analysis revealed that endogenous Regnase-1 was co-precipitated with Myc-tagged 14-3-3 $\epsilon$  as well as with HA-tagged  $\beta$ TRCP in HeLa cells in response to IL-1 $\beta$  stimulation (Figure 1C and Figure 1—figure supplement 1).

As the 14-3-3 family consists of seven paralogs in human and mouse (Aitken, 2006), we investigated the binding of these members to Regnase-1 via immunoprecipitation (Figure 1—figure supplement 2). Among seven of the 14-3-3 proteins, 14-3-3 $\beta$ ,  $\gamma$ , and  $\epsilon$  strongly interacted with Regnase-1, while 14-3-3 $\zeta$ ,  $\eta$ , and  $\theta$  showed weak interaction. Interestingly,

Regnase-1 failed to associate with 14-3-3- $\sigma$ , the latter of which was reported to exclusively form a homodimer but not a heterodimer with other 14-3-3 isoforms (Verdoodt et al., 2006).

To investigate if stimulation with TLR ligands also induces Regnase-1-14-3-3 binding, we stimulated RAW267.4 macrophages stably expressing Myc-14-3-3 $\epsilon$  with Pam<sub>3</sub>CSK<sub>4</sub> (a ligand for TLR1/2), poly I:C (a ligand for TLR3), LPS (a ligand for TLR4), R848 (a ligand for TLR7/8), or CpG DNA (a ligand for TLR9), and immunoprecipitated 14-3-3 $\epsilon$  with an anti-Myc antibody. The Regnase-1-14-3-3 interaction was induced by all TLR ligands tested except for poly I:C (Figure 1D). All TLRs other than TLR3 signal through MyD88, while TLR3 utilizes TRIF as an adaptor to trigger intracellular signaling (Fitzgerald & Kagan, 2020; O'Neill et al., 2013; Takeuchi & Akira, 2010). Considering that IL-1 $\beta$  signal is also dependent on MyD88 (Akira et al., 2006), MyD88-dependent, but not TRIF-dependent, signaling pathways trigger the Regnase-1-14-3-3 binding.

Collectively, these results demonstrate that IL-1R/TLR stimulation induces dynamic remodeling of the Regnase-1-associating protein complex from translation machineries to SCF complexes and/or 14-3-3 proteins.

### **Phosphorylation of Regnase-1 at S494 and S513 is necessary for Regnase-1-14-3-3 binding**

Since 14-3-3 proteins are known to recognize phosphorylated proteins (Muslin et al., 1996), we investigated if 14-3-3-bound Regnase-1 is phosphorylated by inflammatory stimuli. SDS-PAGE analysis revealed that Regnase-1 band migration was slower in samples

stimulated with IL-1 $\beta$  or TLR ligands (except for a TLR3 ligand, poly I:C) - a hallmark of Regnase-1 phosphorylation (Figure 1C–D, 2A, and Figure 2—figure supplement 1) (Iwasaki et al., 2011; Tanaka et al., 2019). Indeed, the mobility change of Regnase-1 was abolished when the cell lysates were treated with  $\lambda$ -protein phosphatase ( $\lambda$ PP) (Figure 2A–B). Furthermore, the Regnase-1 band in the 14-3-3-precipitate migrated slower;  $\lambda$ PP treatment of the 14-3-3-precipitate abolished this phenomenon (Figure 2A–B). Thus, 14-3-3 specifically binds to phosphorylated Regnase-1.

We next scrutinized Regnase-1 phosphorylation sites induced by IL-1 $\beta$  stimulation to identify phosphorylation sites critical for the Regnase-1-14-3-3 interaction. We purified FLAG-HA-Regnase-1 from HeLa cells stimulated with or without IL-1 $\beta$  and identified IL-1 $\beta$ -inducible phosphorylation sites by LC-MS/MS (Figure 2C and Figure 2—figure supplement 2). We found that the phosphorylation at S21, S61, S62, S362, S439, S470, S494, and S513 of Regnase-1 was increased in response to IL-1 $\beta$  stimulation. To identify Regnase-1 phosphorylation sites responsible for binding with 14-3-3, we mutated serine residues on Regnase-1 phosphorylation sites into alanine and probed its association with 14-3-3. Among the Regnase-1-SA mutants, S494A and S513A mutants failed to be co-precipitated with 14-3-3 (Figure 2D), indicating that phosphorylation at both of S494 and S513 is necessary for the Regnase-1-14-3-3 interaction. Both phosphorylation sites harbor a pSxP sequence, which shows similarity with a known 14-3-3 binding motif, RxxpSxP, mode 1 (Yaffe et al., 1997). Noteworthy, amino acid sequences surrounding S494 and S513 are highly conserved among many species (Figure 2E–F).

We next investigated the mechanism of how Regnase-1 phosphorylation is regulated by inflammatory stimuli. In response to IL-1 $\beta$  or TLR ligands stimulation, MyD88 associates with IRAK kinases, IRAK1 and IRAK2, via the death domain (Gottipati et al., 2008; Wesche et al., 1997). A part of C-terminal region of IRAKs in turn interacts with TRAF6 to activate NF- $\kappa$ B (Ye et al., 2002). It was shown that *Irak1* and *Irak2* double deficiency abolished the phosphorylation of Regnase-1 after LPS stimulation (Iwasaki et al., 2011). We found that gene depletion of *IRAK1/2* using the CRISPR-Cas9 system in HeLa cells severely impaired the association between Regnase-1 and 14-3-3 as well as the phosphorylation of Regnase-1 in response to IL-1 $\beta$  stimulation (Figure 2—figure supplement 3). Reciprocally, overexpression of IRAK1 and IRAK2 induced Regnase-1-14-3-3 binding (Figure 2G). In contrast, the interaction between Regnase-1 and 14-3-3 was not induced by the expression of a kinase-inactive mutant (T209A) IRAK1 (Kollewe et al., 2004) or a deletion mutant lacking death domain ( $\Delta$ 1-103) of IRAK1, indicating that the Regnase-1-14-3-3 binding requires the IRAK1 kinase activity as well as recruitment to MyD88 (Figure 2H–I). Although the C-terminal 619-710 portion of IRAK1 was also required for Regnase-1-14-3-3 binding, point mutations in TRAF6 binding sites (E541/E584/E704A) (Ye et al., 2002) did not abolish the Regnase-1-14-3-3 binding (Figure 2H–I). *In silico* prediction suggested the presence of a C-terminal structural domain (CSD) in the 619-710 of IRAK1 (Figure 2—figure supplement 4). In the CSD of IRAK1, highly conserved amino acids, R663 and K665, are critical for the Regnase-1-14-3-3 binding (Figure 2H–I), suggesting that the CSD of IRAK1 controls Regnase-1-14-3-3 interaction irrespective of the recruitment of TRAF6. Of note, the

R663/K665A mutant IRAK1 was capable of activating NF- $\kappa$ B (Figure 2—figure supplement 5), indicating that the IRAK1 C-terminal region has two distinct functions: NF- $\kappa$ B activation through TRAF6 binding sites and the induction of Regnase-1-14-3-3 interaction through the CSD.

S494 and S513 of Regnase-1 are also reported to be phosphorylated by overexpression of Act1 together with TANK-binding kinase 1 (TBK1) or IKK-i/ $\epsilon$ , which mimics IL-17 signaling (Tanaka et al., 2019). We detected phosphorylation at S494 and S513 of Regnase-1 in IL-17A-stimulated cells as well as IL-1 $\beta$ -stimulated cells by LC-MS/MS (Figure 2—figure supplement 6, 7). Furthermore, we found that IL-17A stimulation also induced Regnase-1-14-3-3 binding (Figure 2—figure supplement 8).

Collectively, these data demonstrate that the IRAK-dependent phosphorylation of Regnase-1 at S494 and S513 is necessary for the association between Regnase-1 and 14-3-3.

### **$\beta$ TRCP binds to 14-3-3-free Regnase-1**

MyD88-dependent signaling also induces IKK-mediated phosphorylation of Regnase-1 at S435 and S439, which allows recognition of Regnase-1 by  $\beta$ TRCP (Iwasaki et al., 2011). With this, we examined the relationship between the association of Regnase-1 to 14-3-3 and to  $\beta$ TRCP. We found that Regnase-1 harboring S435A and S439A mutations permitted the interaction with 14-3-3 but failed to recruit  $\beta$ TRCP (Figure 3A–B). Reciprocally, the S494A or S513A mutation of Regnase-1 did not inhibit the association between Regnase-1 and  $\beta$ TRCP (Figure 3B), indicating that the phosphorylation of Regnase-1 at S494 or S513 or the

Regnase-1-14-3-3 binding is dispensable for the Regnase-1- $\beta$ TRCP association. We next compared the phosphorylation status of  $\beta$ TRCP-bound and 14-3-3-bound Regnase-1. Since  $\beta$ TRCP-mediated polyubiquitination potentially alters the molecular weight of Regnase-1, we utilized a  $\beta$ TRCP mutant which is unable to induce polyubiquitination due to the lack of the F-box domain ( $\beta$ TRCP- $\Delta$ F). Interestingly, the SDS-PAGE analysis revealed that  $\beta$ TRCP- $\Delta$ F-bound Regnase-1 migrated faster than 14-3-3-bound Regnase-1 (Figure 3C–D), indicating that  $\beta$ TRCP likely binds to 14-3-3-free Regnase-1.

These results demonstrate that the binding of Regnase-1 to 14-3-3 and  $\beta$ TRCP occurs independently although IL-1 $\beta$  stimulation simultaneously induces phosphorylation of Regnase-1 at S494 and S513 as well as S435 and S439. In addition, 14-3-3 inhibits the Regnase-1- $\beta$ TRCP binding.

### **The S513A mutation destabilizes Regnase-1 protein without affecting target mRNA abundance**

To evaluate the functional roles of Regnase-1-14-3-3 interaction, we generated *Zc3h12a*<sup>S513A/S513A</sup> knock-in mice (Figure 4—figure supplement 1). *Zc3h12a*<sup>S513A/S513A</sup> mice did not show gross abnormality, nor did they exhibit alteration in the numbers of T, B cells or macrophages (data not shown). We stimulated mouse embryonic fibroblasts (MEFs) derived from *Zc3h12a*<sup>WT/WT</sup> and *Zc3h12a*<sup>S513A/S513A</sup> mice with IL-1 $\beta$  and checked Regnase-1 expression (Figure 4A). Immunoblot analysis revealed that Regnase-1 was degraded 30 min after stimulation in both WT and S513A mutant MEFs. Following this, Regnase-1 levels

217 increased in WT MEFs at 2 and 4 hours after stimulation (Figure 4A). Notably, most of the  
 218 newly synthesized Regnase-1 showed slow migration, consistent with the  
 219 immunoprecipitation experiment using HeLa cells or RAW264.7 cells shown in Figure 1C  
 220 and 1D. On the other hand, the slowly migrating Regnase-1 band did not appear in  
 221 *Zc3h12a*<sup>S513A/S513A</sup> MEFs after IL-1 $\beta$  stimulation. Interestingly, the amount of Regnase-1 at  
 222 lower bands, which are not the binding target of 14-3-3 (Figure 2A), was comparable  
 223 between WT and *Zc3h12a*<sup>S513A/S513A</sup> at corresponding time points. Consequently, total  
 224 Regnase-1 protein expression was severely reduced in *Zc3h12a*<sup>S513A/S513A</sup> MEFs compared  
 225 with WT after IL-1 $\beta$  stimulation (Figure 4A). Similar results were also obtained when bone  
 226 marrow-derived macrophages (BMDMs) and thioglycollate-elicited peritoneal exudate cells  
 227 (PECs) derived from *Zc3h12a*<sup>WT/WT</sup> and *Zc3h12a*<sup>S513A/S513A</sup> mice were stimulated with LPS  
 228 (Figure 4B–C). Nevertheless, *Zc3h12a* mRNA levels were comparable between  
 229 *Zc3h12a*<sup>WT/WT</sup> and *Zc3h12a*<sup>S513A/S513A</sup> cells (Figure 4D–F), suggesting that S513A mutation  
 230 affects the protein stability of Regnase-1. To address this, we examined the kinetics of  
 231 Regnase-1 degradation following LPS stimulation by treating cells with cycloheximide  
 232 (CHX). Indeed, Regnase-1-S513A was more rapidly degraded than Regnase-1-WT in PECs  
 233 after LPS stimulation (Figure 4—figure supplement 2). Furthermore, treatment of  
 234 *Zc3h12a*<sup>S513A/S513A</sup> PECs with MG-132, a proteasome inhibitor, resulted in the increase of  
 235 smearing in the band patterns of Regnase-1 in LPS-stimulated cells (Figure 4C), possibly due  
 236 to the inhibition of degradation of polyubiquitinated Regnase-1. These data indicate that the  
 237 phosphorylation of Regnase-1 at S513 stabilizes Regnase-1 protein after IL-1 $\beta$  or LPS



stimulation by binding with 14-3-3.

We next checked whether the altered Regnase-1 expression by the S513A mutation affects Regnase-1-mediated mRNA decay. Despite the huge difference in Regnase-1 expression, the expression of *Il6*, a transcript degraded by Regnase-1 (Figure 4—figure supplement 3), was comparable between *Zc3h12a*<sup>WT/WT</sup> and *Zc3h12a*<sup>S513A/S513A</sup> cells (Figure 4D–I). In addition, the stability of Regnase-1 target mRNAs including *Il6*, *Zc3h12a*, and *Nfkbiz* was equivalent between *Zc3h12a*<sup>WT/WT</sup> and *Zc3h12a*<sup>S513A/S513A</sup> cells (Figure 4—figure supplement 4). Furthermore, even when we analyzed gene expression profile comparing *Zc3h12a*<sup>WT/WT</sup> and *Zc3h12a*<sup>S513A/S513A</sup> macrophages by an RNA-seq analysis (Figure 4—figure supplement 5), we did not identify any differentially expressed genes (adj  $P < 0.05$ ) between *Zc3h12a*<sup>WT/WT</sup> and *Zc3h12a*<sup>S513A/S513A</sup> macrophages irrespective of the stimulation with LPS.

To examine the mechanisms underlying these observations, we developed two mathematical models based on our previous studies (see Materials and Methods) (Iwasaki et al., 2011; Mino et al., 2019). The first model (Model 1) assumes that 14-3-3-bound Regnase-1 is unable to degrade its target mRNAs (Figure 4J). The second model (Model 2) assumes that Regnase-1 binding with 14-3-3 maintains its ability to degrade its target mRNAs to a certain extent (Figure 4K). Mathematical analysis showed that in Model 2, the abundance of the *Il6* mRNAs should be different between *Zc3h12a*<sup>WT/WT</sup> and *Zc3h12a*<sup>S513A/S513A</sup> cells under the condition that the amount of 14-3-3-free Regnase-1 protein (lower bands in Figure 4A–C) is comparable between them. Our observations that

the abundance of the target mRNAs did not differ between *Zc3h12a*<sup>WT/WT</sup> and *Zc3h12a*<sup>S513A/S513A</sup> cells in the late phase of stimulation is inconsistent with Model 2, suggesting that Regnase-1 is inactivated upon binding to 14-3-3.

These results imply that the phosphorylation at S513 and the following association with 14-3-3 nullifies Regnase-1's ability in degrading target mRNAs, although it stabilizes and significantly upregulates the abundance of Regnase-1.

### **14-3-3 inactivates Regnase-1 by inhibiting Regnase-1-RNA binding**

The mathematical analysis suggests that 14-3-3-bound Regnase-1 is inactive as the S513A mutation failed to affect *Il6* expression in MEFs or macrophages. To examine if this comparable *Il6* expression was due to increased degradation of Regnase-1-S513A protein via  $\beta$ TRCP, we further mutated  $\beta$ TRCP-recognition sites, S435 and S439, to alanine in Regnase-1-S513A (Regnase-1-S435/439/513A). As shown in Figure 5A, the Regnase-1-S435/439/513A mutant was more abundantly expressed than Regnase-1-S513A after IL-1 $\beta$  stimulation, indicating that Regnase-1-S513A is degraded via the association with  $\beta$ TRCP. It is noteworthy that most of Regnase-1-S435/439/513A showed fast migration, whereas the majority of Regnase-1-S435/439A migrated slowly in response to the stimulation. To verify if 14-3-3-bound Regnase-1 is functional or not, we assessed the target mRNA suppression activity of each mutant by checking the expression of *Il6* co-transfected with Regnase-1. Regnase-1-S435/439/513A was more potent in suppressing *Il6* expression compared to WT or other SA mutants, S513A and S435/439A, in response to IL-1 $\beta$

stimulation (Figure 5B). These results indicate that IL-1 $\beta$  stimulation regulates the activity of Regnase-1 by two independent mechanisms via 14-3-3 and  $\beta$ TRCP, respectively.

To further examine the mechanism of how 14-3-3 inactivates Regnase-1, we attempted to generate a Regnase-1 mutant which constitutively binds to 14-3-3 even without stimulation. We generated a phospho-mimic mutant of Regnase-1 (S494D/S513D). However, this mutant failed to bind 14-3-3 (Figure 5C), indicating that the phosphate moiety, but not negative charge, is recognized by 14-3-3. Then we utilized a sequence of Exoenzyme S (ExoS), which is a bacterial protein derived from *Pseudomonas aeruginosa* and is known to bind to 14-3-3 without phosphorylation (Fu et al., 1993; Karlberg et al., 2018; Masters et al., 1999). The 22 amino acids of Regnase-1 covering S494 and S513 were substituted with two ExoS (419-429) sequences (Figure 5D). As a control, we additionally mutated Regnase-1-ExoSx2 by substituting its core sequences for 14-3-3 binding (L426, D427, and L428) with alanine residues (Regnase-1-ExoSAAx2) (Ottmann et al., 2007; Yasmin et al., 2006). We observed that Regnase-1-ExoSx2, but not Regnase-1-ExoSAAx2, interacted with endogenous 14-3-3 without any stimulation (Figure 5C). Using these mutants, we investigated whether 14-3-3 binding alters the activity of Regnase-1 to suppress *Il6* expression. Consistent with its 14-3-3 binding capacity, Regnase-1-ExoSx2, but not Regnase-1-ExoSAAx2 and -S494D/S513D, lost the activity to inhibit *Il6* expression (Figure 5E). Furthermore, the production of IL-6 protein was similarly inhibited depending on the capacity of Regnase-1 to bind 14-3-3 (Figure 5F). In addition, Regnase-1-mediated suppression of *Il6* expression was impaired by the overexpression of IRAK1-WT and

E541/E584/E704A mutants, both of which induce Regnase-1-14-3-3 association (Figure 5G). On the other hand, IRAK1 mutants that failed to induce the Regnase-1-14-3-3 association (T209A,  $\Delta$ 1-103,  $\Delta$ 619-710, and R663/K665A) did not affect the activity of Regnase-1.

We next examined how 14-3-3 inhibits the activity of Regnase-1 by investigating Regnase-1-mRNA binding activity using various Regnase-1 mutants in HeLa cells. To stabilize Regnase-1-RNA binding, we generated a nuclease inactive version of Regnase-1 by introducing the D141N mutation to each of Regnase-1 mutant (Matsushita et al., 2009) (Figure 5—figure supplement 1). As shown in Figure 5H, forced interaction of Regnase-1-D141N with 14-3-3 by the ExoSx2 mutation in HeLa cells abrogated the binding with *IL6* mRNA, whereas *IL6* was co-precipitated with Regnase-1-D141N, -ExoSAAx2-D141N and -S494D/S513D-D141N (Figure 5H). In addition to *IL6*, Regnase-1-ExoSx2 failed to bind to other reported target mRNAs such as *NFKBIZ*, *PTGS2*, and CXC chemokines (Figure 5—figure supplement 2). Collectively, these data demonstrate that 14-3-3 inhibits Regnase-1-mRNA binding, thereby abrogating Regnase-1-mediated mRNA degradation.

### **14-3-3 inhibits nuclear import of Regnase-1**

We have previously shown that Regnase-1 interacts with CBP80-bound, but not eIF4E-bound, mRNAs (Mino et al., 2019), indicating that Regnase-1 degrades mRNAs immediately after the export from the nucleus to the cytoplasm (Maquat et al., 2010; Müller-Mcnicoll & Neugebauer, 2013). Although Regnase-1 mainly localizes in the

cytoplasm (Mino et al., 2015), we hypothesized Regnase-1 shuttles between the nucleus and the cytoplasm to recognize its target mRNAs in association with their nuclear export. To test this hypothesis, we examined the subcellular localization of Regnase-1 following the treatment with Leptomycin B (LMB), which inhibits CRM1 (also known as Exportin-1)-mediated protein export from the nucleus to the cytoplasm (Yashiroda & Yoshida, 2005). Whereas Regnase-1 localized in the cytoplasm in the steady state condition, LMB treatment induced rapid accumulation of Regnase-1 in the nucleus within 30 minutes (Figure 6A). These results suggest that Regnase-1 dynamically changes its localization between the cytoplasm and the nucleus. Given that Regnase-1 dominantly localizes in the cytoplasm in the steady state conditions, the frequency of its nuclear export seems to be higher than its nuclear import.

CRM1 is known to recognize a nuclear export signal (NES) of a cargo protein for the protein export (Hutten & Kehlenbach, 2007). Thus, we investigated if Regnase-1 harbors a NES. *In silico* prediction deduced amino acids 433-447 of Regnase-1 as a potential NES with high probability (Xu et al., 2015) (Figure 6B–D). Indeed, Regnase-1 lacking 422-451 spontaneously accumulated in the nucleus (Figure 6E). Since NESs are characterized by hydrophobic residues (la Cour et al., 2003), we also inspected which hydrophobic residues of Regnase-1 were important for the efficient nuclear export of Regnase-1. We found that L440, M444, L447, and W448 of Regnase-1 were critical for the nuclear export of Regnase-1 (Figure 5E). Noteworthy, all the residues are highly conserved among species (Figure 5D).

We next examined whether 14-3-3 binding controls the localization of Regnase-1.

343 Interestingly, Regnase-1-ExoSx2 failed to accumulate in the nucleus even after LMB  
344 treatment while Regnase-1-WT and -ExoSAAx2 accumulated in the nucleus by LMB  
345 treatment (Figure 6F). This result indicates that Regnase-1-ExoSx2 is unable to translocate  
346 into the nucleus like Regnase-1-WT. Taken together, 14-3-3 inhibits the nuclear import of  
347 Regnase-1 as well as its binding to target mRNAs.

348

## Discussion

In the present study, we discovered that IL-1 $\beta$  and TLR stimulation dynamically changes protein-protein interaction of Regnase-1. Particularly, these stimuli trigger the interaction of Regnase-1 with 14-3-3 as well as  $\beta$ TRCP via phosphorylation at distinct amino acids. Whereas phosphorylation of Regnase-1 at S494 and S513 is recognized by 14-3-3,  $\beta$ TRCP associates with Regnase-1 phosphorylated at S435 and S439. We demonstrated that each Regnase-1-14-3-3 and Regnase-1- $\beta$ TRCP binding occurs independently. Furthermore, 14-3-3 prevent Regnase-1- $\beta$ TRCP binding, resulting in protein stabilization of 14-3-3-bound Regnase-1.

The amino acid sequence surrounding S494 and S513 of Regnase-1 is widely conserved among species. Particularly, both S494 and S513 harbor the pSxP sequence motif, which overlaps with a known 14-3-3 binding motif, RxxpSxP, mode 1 (Yaffe et al., 1997). It is quite plausible that the 14-3-3 dimer directly binds to phosphorylated S494 and S513 of Regnase-1 with the phospho-peptide binding groove. Interestingly, only 14-3-3 $\sigma$ , which forms a homodimer but not a heterodimer with other 14-3-3 isoforms (Verdoodt et al., 2006), failed to bind with Regnase-1 (Figure 1—figure supplement 2). This result might be a clue to elucidate the target specificity of each 14-3-3 paralog.

14-3-3 and  $\beta$ TRCP inhibit Regnase-1-mediated mRNA decay via distinct mechanisms; 14-3-3 prevents Regnase-1-mRNA binding while  $\beta$ TRCP induces protein degradation of Regnase-1. Analysis of *Zc3h12a*<sup>S513A/S513A</sup> mice revealed that 14-3-3-mediated abrogation of Regnase-1 can be compensated by the degradation of

Regnase-1. The presence of this dual regulatory system underscores the importance of restricting the activity of Regnase-1 to ensure proper inflammatory gene expression when cells encounter PAMPs or DAMPs (Figure 6G).

Notably, exome sequence analysis of the colon samples from ulcerative colitis patients discovered mutations in the  $\beta$ TRCP binding site of Regnase-1 (Kakiuchi et al., 2020; Nanki et al., 2020). Furthermore, a previous report showed that *Zc3h12a*<sup>S435/S439A</sup> mutant mice were resistant to experimental autoimmune encephalomyelitis (EAE) (Tanaka et al., 2019). All these mutations abolish  $\beta$ TRCP-mediated degradation of Regnase-1. However, genetic association between the 14-3-3-binding site of Regnase-1 and inflammatory diseases has not been identified so far. This is possibly because of the compensation by  $\beta$ TRCP-mediated regulation, which we observed in *Zc3h12a*<sup>S513A/S513A</sup> mice and HeLa cells transiently expressing Regnase-1-S513A and S435/439/513A. Previous studies have shown that viral proteins or lncRNAs inhibit  $\beta$ TRCP-mediated protein degradation (Guo et al., 2020; Neidel et al., 2019; van Buuren et al., 2014; Yang et al., 2020). 14-3-3-mediated regulation of Regnase-1 may serve as a backup mechanism to control the activity of Regnase-1 when  $\beta$ TRCP-mediated protein degradation is dysregulated.

While  $\beta$ TRCP regulates the abundance of Regnase-1 through protein degradation, 14-3-3 regulates the activity of Regnase-1. We found that 14-3-3-bound Regnase-1 failed to associate with mRNAs, indicating that 14-3-3 prevents Regnase-1 from recognizing target mRNA. We have previously shown that an RNase domain and an adjacent zinc finger domain play an important role in Regnase-1-RNA binding (Yokogawa et al., 2016). However,



the 14-3-3-binding site of Regnase-1 is in the C-terminal part of Regnase-1, which is distant from RNase and zinc finger domains. Therefore, 14-3-3 is unlikely to inhibit Regnase-1-mRNA binding by simple competition between 14-3-3 and mRNAs for the RNA binding domain of Regnase-1. We have previously reported that Regnase-1 interacts with CBP80-bound, but not eIF4E-bound, mRNAs, indicating that Regnase-1 recognizes its target mRNA before or immediately after the nuclear export of the mRNA (Mino et al., 2019). In this study, we found that Regnase-1 shuttles between the nucleus and the cytoplasm while 14-3-3-bound Regnase-1 cannot enter the nucleus. Thus, it is tempting to speculate that Regnase-1 recognizes mRNA in the nucleus and induce mRNA decay during pioneer rounds of translation immediately after the nuclear export (Maquat et al., 2010; Müller-Mcnicoll & Neugebauer, 2013). Nevertheless, further investigation is required to clarify the mechanisms of Regnase-1-mediated mRNA decay depending on its nuclear-cytoplasmic shuttling. In addition, further studies are also necessary to clarify the molecular mechanisms how 14-3-3 controls the nuclear-cytoplasmic shuttling of Regnase-1 as well as how it regulates Regnase-1-mRNA binding by exploiting systems beyond the ExoS sequence-mediated interaction with 14-3-3.

$\beta$ TRCP is likely to recognize 14-3-3-free Regnase-1, indicating that 14-3-3 inhibits Regnase-1- $\beta$ TRCP interaction. There are two possible mechanisms to explain this. One posits that 14-3-3 bound to phosphorylated S494 and S513 of Regnase-1 conceals  $\beta$ TRCP-binding site (pS435 and pS439), although the 14-3-3-binding site does not overlap with  $\beta$ TRCP-binding site completely. The other possible explanation is that 14-3-3-mediated

inhibition of nuclear-cytoplasmic shuttling of Regnase-1 controls  $\beta$ TRCP-mediated Regnase-1 degradation. Indeed,  $\beta$ TRCP localizes not only in the cytoplasm, but also in the nucleus (Davis et al., 2002). It is plausible that 14-3-3 prevents Regnase-1- $\beta$ TRCP interaction in the nucleus, by inhibiting nuclear-cytoplasmic shuttling of Regnase-1. Of note, the NES of Regnase-1 is located just adjacent to  $\beta$ TRCP-binding site (Figure 6C–D), implying possibility of competitive binding of  $\beta$ TRCP and CRM1 to Regnase-1.

Among the molecules involved in MyD88-dependent signaling, we found that IRAK1/2 are potent inducers of the interaction between Regnase-1 and 14-3-3, thereby abrogating Regnase-1-mediated mRNA decay. We also found that kinase-inactive IRAK1 failed to induce the Regnase-1-14-3-3 complex, suggesting that the kinase activity of IRAK1 is required for the phosphorylation of Regnase-1 at S494 and S513. However, previously identified substrate sequence motifs of IRAK1, pSxV and KxxxpS (Sugiyama et al., 2019) do not match the sequence surrounding S494 and S513 of Regnase-1 (Figure 2F). Although the motif analysis does not exclude the possibility of direct phosphorylation of Regnase-1 by IRAK1, it is possible that kinases activated by IRAK1/2 phosphorylates Regnase-1 at S494 and S513.

IRAKs are involved in stabilization of inflammatory mRNAs as well as NF- $\kappa$ B activation (Flannery et al., 2011; Hartupée et al., 2008; Wan et al., 2009). A previous study showed that IRAK1-mediated mRNA stabilization does not require IRAK1-TRAF6 association (Hartupée et al., 2008). Interestingly, the IRAK1-TRAF6 association is also dispensable for the Regnase-1-14-3-3 binding. Instead, other evolutionarily conserved amino

acids in the C-terminal structural domain (CSD) of IRAK1, R663 and K665, are critical for  
Regnase-1-14-3-3 binding. Considering 14-3-3-mediated inactivation of Regnase-1, it is  
plausible that the CSD of IRAK1 is the key for stabilization of inflammatory mRNAs.

In summary, Regnase-1 interactome analysis revealed dynamic 14-3-3-mediated  
regulation of Regnase-1 in response to IL-1 $\beta$  and TLR stimuli. Since recent studies identified  
Regnase-1 as a high-potential therapeutic target in various diseases (Kakiuchi et al., 2020;  
Nanki et al., 2020; Wei et al., 2019), our findings may help maximize the effect of Regnase-1  
modulation or provide an alternative way to control the activity of Regnase-1.

## 442 Materials and Methods

Key Resources Table				
Reagent type (species) or resource	Designation	Source or reference	Identifiers	Additional information
gene ( <i>Mus musculus</i> )	<i>Zc3h12a</i>	NA	Gene ID: 230738	
gene ( <i>Homo sapiens</i> )	<i>ZC3H12A</i>	NA	Gene ID: 80149	
strain, strain background ( <i>Mus musculus</i> )	<i>Zc3h12a</i> <sup>WT/WT</sup>	CLEA Japan	C57BL/6	C57BL/6JJcl
strain, strain background ( <i>Mus musculus</i> )	<i>Zc3h12a</i> <sup>-/-</sup>	<a href="https://doi.org/10.1038/nature07924">https://doi.org/10.1038/nature07924</a>		
strain, strain background ( <i>Mus musculus</i> )	<i>Zc3h12a</i> <sup>S513A/S513A</sup>	this paper		generated using CRISPR-Cas9 system
sequence-based reagent	DNA oligo (for pX330)	this paper	CACCGCGGCT CAGACCAGTA CTCTC	for <i>Zc3h12a</i> <sup>S513A/S513A</sup> generation
sequence-based reagent	DNA oligo (for pX330)	this paper	AAACGAGAGT ACTGGTCTGA GCCGC	for <i>Zc3h12a</i> <sup>S513A/S513A</sup> generation
sequence-based reagent	donor single strand oligo	this paper	GAAGGACAGG AGTGGGTGG GGGTAATGGG TACGGCTCAG CCCAGTACTC TCTGGATGGG TAGGTGGGTG GCGGGGGCA CA	for <i>Zc3h12a</i> <sup>S513A/S513A</sup> generation
sequence-based reagent	DNA oligo (for pX459- <i>IRAK1KO</i> )	<a href="https://doi.org/10.1093/bioinformatics/btu743">https://doi.org/10.1093/bioinformatics/btu743</a>	CACCGGTCTG GTCGCGCACG ATCA	
sequence-based reagent	DNA oligo (for pX459- <i>IRAK1KO</i> )	<a href="https://doi.org/10.1093/bioinformatics/btu743">https://doi.org/10.1093/bioinformatics/btu743</a>	AAACTGATCG TGCGCGACCA GACC	

sequence-based reagent	DNA oligo (for pX459- <i>IRAK2KO</i> )	<a href="https://doi.org/10.1038/nbt.3437">https://doi.org/10.1038/nbt.3437</a>	CACCGAAAAC CGCAAAATCA GCCAG	
sequence-based reagent	DNA oligo (for pX459- <i>IRAK2KO</i> )	<a href="https://doi.org/10.1038/nbt.3437">https://doi.org/10.1038/nbt.3437</a>	AAACCTGGCT GATTTTGC GG TTTTC	
antibody	anti-mouse-Regnase-1 (rabbit polyclonal)	MBL life science		custom antibody production (1:1000)
antibody	anti-human-Regnase-1 (rabbit polyclonal)	Atlas Antibodies	Cat # HPA032053	(1:500)
antibody	anti-14-3-3 (pan) (mouse monoclonal)	Santa Cruz Biotechnology	Cat # sc-1657	(1:1000)
antibody	anti-I $\kappa$ B- $\alpha$ (rabbit polyclonal)	Santa Cruz Biotechnology	Cat # sc-371	(1:1000)
antibody	anti-IRAK1 (mouse monoclonal)	Santa Cruz Biotechnology	Cat # sc-5288	(1:500)
antibody	anti-FLAG (mouse monoclonal)	Sigma	Cat # F3165	(WB:1:2000, IF:1:5000)
antibody	anti-FLAG (rabbit polyclonal)	Sigma	Cat # F7425	(1:2000)
antibody	anti-HA (mouse monoclonal)	Sigma	Cat # H3663	(1:2000)
antibody	anti-HA (rabbit polyclonal)	Sigma	Cat # H6908	(1:2000)
antibody	anti-Myc (mouse monoclonal)	Sigma	Cat # M4439	(1:2000)
antibody	anti-Myc (rabbit polyclonal)	Sigma	Cat # C3956	(1:2000)

antibody	anti- $\beta$ -Actin-HRP (mouse monoclonal)	Santa Cruz Biotechnology	Cat # sc-47778-HRP	(1:2000)
antibody	Anti-Mouse IgG-HRP F(ab') <sub>2</sub> (sheep polyclonal)	cytiva	Cat # NA9310-1ML	(1:5000)
antibody	Anti-Rabbit IgG-HRP F(ab') <sub>2</sub> (donkey polyclonal)	cytiva	Cat # NA9340-1ML	(1:5000)
antibody	F(ab') <sub>2</sub> -anti-Mouse IgG (H+L)-AF488 (Goat polyclonal)	Invitrogen	Cat # A11017	(1:2000)
recombinant DNA reagent	pX330-U6-Chimeric_BB-CBh-hSpCas9	Addgene	RRID:Addgene_42230	
recombinant DNA reagent	pSpCas9(BB)-2A-Puro (PX459) V2.0	Addgene	RRID:Addgene_62988	
recombinant DNA reagent	pMD2.G	Addgene	RRID:Addgene_12259	
recombinant DNA reagent	pMDLg/pRRE	Addgene	RRID:Addgene_12251	
recombinant DNA reagent	pRSV-Rev	Addgene	RRID:Addgene_12253	
recombinant DNA reagent	pInducer20	Addgene	RRID:Addgene_44012	
recombinant DNA reagent	pInducer20-puro	this paper		NeoR of pInducer20 (Addgene_44012) was replaced with PuroR
recombinant DNA reagent	pFLAG-CMV2	Sigma	Cat # E7033	
recombinant DNA reagent	pEGFP-C1	Clontech		
peptide, recombinant protein	FLAG Peptide	Sigma	Cat # F3290	

peptide, recombinant protein	HA peptide	MBL Life science	Cat # 3320	HA tagged Protein PURIFICATION KIT
peptide, recombinant protein	recombinant human IL-1 $\beta$	R&D Systems	Cat # 201-LB-005	
peptide, recombinant protein	recombinant mouse IL-1 $\beta$	BioLegend	Cat # 575102	
peptide, recombinant protein	recombinant human IL-17A	BioLegend	Cat # 570502	
peptide, recombinant protein	recombinant human TNF	BioLegend	Cat # 570104	
commercial assay or kit	Dynabeads Protein G	Invitrogen	Cat # 10004D	
commercial assay or kit	Lambda Protein Phosphatase	NEB	Cat # P0753S	
commercial assay or kit	Signal Enhancer HIKARI	nacalai tesque	Cat # 02270-81	
commercial assay or kit	Immobilon Forte Western HRP Substrate	Millipore	Cat # WBLUF0500	
commercial assay or kit	TRIzol Reagent	Invitrogen	Cat # 15596018	
commercial assay or kit	RNA Clean & Concentrator-5	Zymo Research	Cat # R1014	
commercial assay or kit	PowerUp SYBR Green Master Mix	Applied Biosystems	Cat # A25742	
commercial assay or kit	IL-6 Mouse Uncoated ELISA Kit	Invitrogen	Cat # 88-7064-88	
chemical compound, drug	DSP (dithiobis(succin imidyl propionate))	TCI	Cat # D2473	
chemical compound, drug	Pam3CSK4	InvivoGen	Cat # tlrl-pms	
chemical compound, drug	poly I:C	cytiva	Cat # 27473201	
chemical compound, drug	LPS	InvivoGen	Cat # tlrl-smlps	

chemical compound, drug	R848	InvivoGen	Cat # tlrl-r848-5	
chemical compound, drug	CpG DNA	InvivoGen	Cat # tlrl-1668-1	ODN 1668
chemical compound, drug	MG-132	Sigma	Cat # 474790	
chemical compound, drug	Actinomycin D	Sigma	Cat # A9415	
chemical compound, drug	Leptomycin B	Sigma	Cat # L2913	

## Mice

*Zc3h12a*-deficient mice have been described previously (Matsushita et al., 2009). *Zc3h12a*<sup>S513A/S513A</sup> knock-in mice were generated using CRISPR/Cas9-mediated genome-editing technology as previously described (Fujihara & Ikawa, 2014). Briefly, a pair of complementary DNA oligos was annealed and inserted into pX330 (Addgene plasmid # 42230) (Cong et al., 2013). The plasmid was injected together with the donor single strand oligo into fertilized eggs of C57BL/6J mice. Successful insertion was confirmed by direct sequencing.

All mice were grown under specific pathogen-free environments. All animal experiments were conducted in compliance with the guidelines of the Kyoto University animal experimentation committee (Approval number: MedKyo21057).

## Reagents

Recombinant cytokines, TLR ligands, and chemical compounds were listed in the key resources table.

## Cell culture

HeLa cells, HEK293T cells, RAW264.7 cells, and MEFs were maintained in DMEM



(nacalai tesque) with 10 % fetal bovine serum (FBS), 1 % Penicillin/Streptomycin (nacalai tesque), and 100  $\mu$ M 2-Mercaptoethanol (nacalai tesque). Mycoplasma contamination was routinely tested and found negative.

For the preparation of bone marrow-derived macrophages (BMDMs), bone marrow cells were cultured in RPMI-1640 (nacalai tesque) with 10 % FBS, 1 % Penicillin/Streptomycin, 100  $\mu$ M 2-mercaptoethanol, and 20 ng/ml of macrophage colony-stimulating factor (M-CSF) (BioLegend) for 6 days.

For the preparation of thioglycolate-elicited peritoneal exudate cells (PECs), mice were intraperitoneally injected with 2 ml of 4% (w/v) Brewer's thioglycollate medium. 3.5 days after the injection, peritoneal macrophages were collected and cultured in RPMI-1640 with 10 % FBS, 1 % Penicillin/Streptomycin, and 100  $\mu$ M 2-mercaptoethanol.

#### **Plasmids**

For the expression of FLAG-tagged proteins, pFLAG-CMV2 (Sigma) was used as a backbone. For the expression of HA- or Myc-tagged proteins, the FLAG sequence of pFLAG-CMV2 was replaced by HA- or Myc-sequence. Mouse *Zc3h12a* cDNA was inserted into these vectors as previously described (Matsushita et al., 2009). The coding sequences of 14-3-3 and  $\beta$ TRCP were amplified by using cDNAs derived from HeLa cell as templates and inserted into vectors above using In-Fusion HD Cloning Kit (Takara Bio). For Myc-IRAK1 expression vector, coding sequence of IRAK1 derived from HA-IRAK1 expression vector (Iwasaki et al., 2011) was used. For the mouse *Il6* expression vector, the EGFP sequence in pEGFP-C1 was replaced with *Il6* gene.

Deletions or point mutations were introduced using the QuikChange Lightning Site-Directed Mutagenesis Kit (Agilent) or In-Fusion HD Cloning Kit.

For the lentiviral packaging vectors, pInducer20 (Addgene plasmid #44012) (Meerbrey et al., 2011) was modified to generate pInducer20-puro. FLAG-HA-Regnase-1 sequence was inserted into pInducer20-puro using In-Fusion HD Cloning Kit.

For the Cas9 and gRNA expression plasmids (pX459-IRAK1 and pX459-IRAK2), pX459 (Addgene Plasmid #62988) was digested at BbsI sites, and the annealed oligo coding guide sequence (key resources table) was inserted.

#### **Plasmid transfection**

Plasmids were transfected to HeLa cells or HEK293T cells using Lipofectamine 2000 (Invitrogen) or PEI max (Polysciences) respectively according to manufacturer's instructions.

#### **Generation of doxycycline-inducible FLAG-HA-Regnase-1-expressing HeLa cells**

HeLa cells expressing FLAG-HA-Regnase-1 in a doxycycline-dependent manner were generated by lentiviral transduction. To produce lentivirus, HEK293T cells were transfected with pInducer20-puro-FLAG-HA-Regnase1 together with third generation lentiviral packaging vectors. 6 hours after the transfection, the medium was changed to fresh medium and then the cells were incubated at 37 °C for 48 hours. After the incubation, the medium containing lentivirus was harvested and filtrated through 0.45 µm filter. HeLa cells were incubated with the virus-containing medium at 37 °C for 24 hours, followed by 48-hour-incubation with fresh medium. The transduced cells were selected by 0.5 µg/ml of

puromycin (InvivoGen). Single clones were picked and evaluated for their expression of FLAG-HA-Regnase-1 in a dox-dependent manner by immunoblotting.

#### **Knockout of *IRAK1* and *IRAK2***

HeLa cells were transfected with two pX459 plasmids which contains gRNA sequence for *IRAK1* and *IRAK2*. As the negative control, empty pX459 plasmid was transfected. 48 hours after the pX459 transfection, puromycin (2 µg/ml) was added to the medium. After 48-hour selection with puromycin, the same number of cells were seeded to new dishes and incubated in fresh media without antibiotics for 48 hours. Knockout efficiency was check by immunoblotting using WCL samples.

#### **DSP-crosslinking**

Doxycycline-inducible FLAG-HA-Regnase-1-expressing HeLa cells were treated with doxycycline (1 µg/ml, Sigma) and incubated at 37 °C for 4 hours before the DSP-crosslinking. As a negative control, cells were incubated without doxycycline, and for the IL-1β-stimulated sample, cells were stimulated with human IL-1β (10 ng/ml, R&D Systems) 2 hours before the crosslinking. After the incubation, cells were washed twice with pre-warmed PBS, and then incubated in PBS containing 0.1 mM DSP (TCI) at 37 °C for 30 minutes. After crosslinking, cells were washed once with pre-warmed PBS and incubated in STOP solution (PBS containing 1 M Tris-HCl pH 7.4) at room temperature for 15 minutes. Cells were then washed with ice-cold PBS twice, followed by cell lysis and immunoprecipitation.

## **Immunoprecipitation**

Before immunoprecipitation, pre-washed Dynabeads Protein G (Invitrogen) were incubated with either anti-FLAG antibody (Sigma), anti-HA antibody (Sigma), or anti-Myc antibody (Sigma) at 4 °C with rotation for 1 hour.

For DSP-crosslinked samples, cells were lysed in IP buffer (20 mM Tris-HCl pH 7.4, 150 mM NaCl, and 0.5 % (vol/vol) NP-40) with cOmplete Mini EDTA-free (Sigma), PhosSTOP (Sigma), and 200 U/ml of Benzonase (Millipore) and incubated on ice for 10 minutes. The lysates were centrifuged at 15,000 rpm for 5 minutes and the supernatants were incubated with anti-FLAG-antibody-bound Dynabeads at 4 °C with rotation for 2 hours. The beads were then washed with IP buffer three times and incubated in FLAG-elution buffer (100 µg/ml FLAG peptides (Sigma), 50 mM Tris-HCl pH7.4, and 150 mM NaCl) at 4 °C with rotation for 10 minutes twice. Eluted proteins were then immunoprecipitated using anti-HA-antibody-bound Dynabeads at 4 °C with rotation for 2 hours. After the second immunoprecipitation, the beads were washed three times with IP buffer and the proteins were eluted in Urea elution buffer (8 M Urea and 50 mM Tris-HCl pH 8.0). The samples were stored at -80 °C until trypsin digestion. Proteins were reduced with 10 mM dithiothreitol (Fujifilm Wako) for 30 min, alkylated with 50 mM iodoacetamide (Fujifilm Wako) for 30 min in the dark, diluted 4-fold with 50 mM ammonium bicarbonate (ABC) buffer, and then trypsin digestion was performed. After overnight incubation, digestion was stopped by adding trifluoroacetic acid (TFA) (Fujifilm Wako) to a final concentration of 0.5%. The peptide mixture solution was desalted with SDB-XC StageTips (Rappsilber et al., 2007). The

eluates were dried and resuspended in 200 mM 2-[4-2(2-hydroxyethyl)-1-piperazine]ethanesulfonic acid (HEPES) pH 8.5, mixed with 0.1 mg of TMT10-plex labeling reagents (Thermo Fisher Scientific) dissolved in 5  $\mu$ L acetonitrile (ACN), and incubated for 1 h at room temperature. The reaction mixtures were quenched by adding hydroxylamine (Sigma) to give a final concentration of 0.33%. After 15 minutes incubation, the samples were acidified with trifluoroacetic acid, diluted to 5% ACN, and desalted using SDB-XC StageTips. Peptides were dried, resolved in 5 mM ABC buffer and fractionated with a C18-StageTip. Peptides were eluted with 5 mM ABC containing acetonitrile (12.5%, 15%, 17.5% 20%, 22.5% and 80%) in step gradient manner. Totally 6 fractions were obtained and analyzed by LC/MS/MS.

For the identification of phosphorylation sites of Regnase-1, HeLa cells expressing FLAG-HA-Regnase-1 or FLAG-Regnase-1 were stimulated with IL-1 $\beta$  (10 ng/ml) or IL-17A (50 ng/ml) respectively for 4 hours. The cells were washed with ice-cold PBS twice and lysed in IP buffer with cOmplete Mini EDTA-free and PhosSTOP. Regnase-1 was immunoprecipitated using anti FLAG antibody as described above and eluted from Dynabeads in SDS sample buffer (50 mM Tris-HCl pH 6.8, 2% (wt/vol) SDS, 15% (vol/vol) 2-mercaptoethanol, 10% (vol/vol) glycerol and bromophenol blue), followed by incubation at 95°C for 5 minutes. Regnase-1 was isolated by electrophoresis and the pieces of the gel containing Regnase-1 was stored at 4 °C until trypsin digestion. The gels were de-stained for 30 min with 200  $\mu$ L of 50 mM ABC / 50% ACN. Then the gels were dehydrated by the addition of 100% ACN. Proteins were reduced with 500  $\mu$ L of 10 mM dithiothreitol / 50 mM

ABC for 30 min, alkylated with 50 mM iodoacetamide / 50 mM ABC for 30 min in the dark. The gels were washed two times with 200  $\mu$ L of 0.5% acetic acid / 50% methanol. After washing, gels were re-equilibrated with 50 mM ABC, and subsequently dehydrated by the addition of 100% ACN. 10  $\mu$ L of trypsin solution (10 ng/ $\mu$ L in 50 mM ABC) was added to gel pieces and incubated for 5 min. Another 50  $\mu$ L of 50 mM ABC buffer was added to gel samples and incubated at 37 °C for overnight. After that, elastase (Promega) (150 ng/ $\mu$ L in water) was added to the final concentration of 7.5 ng/ $\mu$ L and incubated for 30 min at 37 °C (Dau et al., 2020). Digestion was stopped by the addition of 5  $\mu$ L of 10% TFA. The supernatants were recovered into fresh Eppendorf tubes, and two additional extraction steps were performed with 50% ACN / 0.1% TFA and 80% ACN / 0.1% TFA. The peptides in the supernatants were dried, resuspended in 0.1% TFA, and desalted using SDB-XC StageTips.

For detecting protein-protein binding, cells were lysed in IP Buffer with cOmplete Mini EDTA-free and PhosSTOP and immunoprecipitated as described above using indicated antibodies. The proteins were eluted in the mixture of IP Buffer and SDS sample buffer (2:1) and incubated at 95°C for 5 minutes.

For detecting protein-RNA binding, cells were lysed in IP Buffer with cOmplete Mini EDTA-free and RNaseOut (Invitrogen) and immunoprecipitated as described above using indicated antibodies. Some of the precipitates were eluted in the mixture of IP Buffer and SDS sample buffer (2:1) to elute proteins and the others were eluted in TRIzol Reagent (Invitrogen) for RNA isolation.

## **LC-MS/MS**

LC/MS/MS analyses were performed with an Orbitrap Fusion Lumos (Thermo Fisher Scientific) connected to an Ultimate 3000 pump (Thermo Fisher Scientific) and an HTC-PAL autosampler (CTC analytics). Peptides were separated by a self-pulled needle column (150 mm length, 100  $\mu$ m ID, 6  $\mu$ m needle opening) packed with Reprosil-Pur 120 C18-AQ 3  $\mu$ m reversed-phase material (Dr. Maisch GmbH), using a 20 min or 65 min gradient of 5–40% B (mobile phase A: 0.5% acetic acid, mobile phase B: 0.5% acetic acid / 80% acetonitrile) at a flow rate of 500 nL/min. The applied ESI voltage was 2.4 kV. For TMT labeled samples, the following parameters were applied: MS scan range of 375–1500, MS1 orbitrap resolution of 120,000, quadrupole isolation window of 0.7, HCD (higher-energy collision dissociation) collision energy of 38%, MS2 orbitrap resolution of 50,000, AGC target value of 50000. For non-labeled samples, the following parameters were applied: MS scan range of 300–1500, MS1 orbitrap resolution of 120,000, quadrupole isolation window of 1.6, HCD collision energy of 30%, MS2 orbitrap resolution of 15,000, MS2 AGC target value of 50000.

## **Database searching and data processing**

For DSP-crosslinked samples, peptides were identified with Mascot version 2.6.1 (Matrix Science) against the sequence of Mouse Regnase-1 in addition to the human database from UniprotKB/Swiss-Prot release 2017/04 and with a precursor ion mass tolerance of 5 ppm and a product ion mass tolerance of 20 ppm. Carbamidomethyl (C), TMT6plex (K) and TMT6plex (N-term) were set as a fixed modification, oxidation (M) was allowed as a variable modification, and up to 2 missed cleavages are allowed with strict Trypsin/P

specificity. Identified peptides were rejected if the Mascot score was below the 95% confidence limit based on the identity score of each peptide. The quantification of peptides was based on the TMT reporter ion intensities in MS2 spectra. Protein quantitative values were calculated by summing the corresponding peptide intensity values. Only proteins with at least two unique peptides were used for further analysis.

For the identification of phosphorylation sites of Regnase-1, peptides were identified with Mascot version 2.7.0 against the sequence of mouse Regnase-1 with a precursor ion mass tolerance of 5 ppm and a product ion mass tolerance of 20 ppm. Carbamidomethyl (C) was set as a fixed modification, oxidation (M) and phosphorylation (STY) were allowed as variable modifications, and up to 2 missed cleavages are allowed with semitrypsin specificity. Identified peptides were rejected if the Mascot score was below the 99% confidence limit based on the identity score of each peptide. The label-free quantification of peptides was based on the peak area in the extracted ion chromatograms using Skyline-daily software version 21.0.9.118 (MacLean et al., 2010). The peak area ratios between stimulated and non-stimulated samples were calculated, log-scaled, and normalized by the median. For quantitation of phosphosites, the peak area ratios of all monophosphopeptides containing the phosphosites of interest were averaged. Phosphosite localization was evaluated with a site-determining ion combination method based on the presence of site-determining y- or b-ions in the peak lists of the fragment ions, which supported the phosphosites unambiguously (Nakagami et al., 2010).

Protein-protein interaction network of the Regnase-1-associating proteins (Log<sub>2</sub> fold



change over negative control > 2) was analyzed using STRING database (Szklarczyk et al., 2019) and visualized in Cytoscape (Shannon et al., 2003). Keratins contaminated in the samples were omitted from the analysis.

#### **$\lambda$ -protein phosphatase ( $\lambda$ PP) treatment**

HeLa cells transiently expressing HA-14-3-3 $\epsilon$  were stimulated with or without IL-1 $\beta$  (10 ng/ml) for 4 hours and lysed in IP Buffer. Some of the lysates were used in immunoprecipitation as described above. The proteins were eluted using 250  $\mu$ g/ml of HA peptides as described above. The lysate and the precipitates were treated with Lambda Protein Phosphatase (NEB) according to manufacturer's instructions. For the  $\lambda$ PP negative samples, the same amount of IP Buffer was added instead of  $\lambda$ PP.

#### **Immunoblotting**

Cells were lysed in IP Buffer or RIPA buffer (1% (vol/vol) NP-40, 0.1% (wt/vol) SDS, 1% (wt/vol) sodium deoxycholate, 150 mM NaCl, 20 mM Tris-HCl pH 8.0, and 10 mM EDTA) with cOmplete Mini EDTA-free and PhosSTOP. The lysates were incubated on ice for 5 minutes and centrifuged at 15,000 rpm for 5 minutes. The supernatants were mixed with SDS sample buffer (2:1) and incubated at 95°C for 5 minutes. SDS-PAGE was performed using e-PAGEL 7.5% or 5~20%(ATTO) and the proteins were transferred onto 0.2  $\mu$ m pore size Immun-Blot PVDF membranes (Bio-Rad), followed by blocking with 5 % skim milk. The antibodies used in immunoblotting were listed in the key resources table. Luminescence was detected with Amersham Imager 600 (cytiva) and the images were analyzed with Fiji (Schindelin et al., 2012).

**RNA isolation and RT-qPCR**

Cells were lysed in TRIzol Reagent, and the RNA was isolated according to manufacturer's instructions. For the isolation of the RNA precipitated with Regnase-1, RNA was isolated using RNA Clean & Concentrator-5 (Zymo Research). RNA was reverse transcribed by using ReverTra Ace (TOYOBO). cDNA was amplified by using PowerUp SYBR Green Master Mix (Applied Biosystems) and measured with StepOnePlus Real-Time PCR System (Applied Biosystems). To analyze mRNA expression, each RNA level was normalized with 18S or ACTB. The primers used in qPCR were listed in Supplementary File 1.

**RNA Sequencing**

PECs were harvested from *Zc3h12a*<sup>WT/WT</sup> and *Zc3h12a*<sup>S513A/S513A</sup> mice as described above. PECs were stimulated with LPS (100 ng/ml) for indicated time and the RNA was collected and isolated using TRIzol Reagent. cDNA library was prepared using NEBNext Ultra RNA Library Prep Kit for Illumina (NEB) and sequenced on NextSeq 500 System (Illumina) according to the manufacturer's instructions. Acquired data was analyzed using Galaxy (Afgan et al., 2018). Briefly, identified reads were mapped on the murine genome (mm10) using HISAT2 (paired end, unstranded) (Galaxy Version 2.1.0), and the mapped reads were counted using featureCounts (Galaxy Version 1.6.3).

**ELISA**

Cytokine concentration was measured by using IL-6 Mouse Uncoated ELISA Kit (Invitrogen) according to manufacturer's instructions. Luminescence was detected with iMark Microplate Reader (Bio-Rad).

## Luciferase assay

5xNF- $\kappa$ B firefly luciferase reporter vector, Renilla luciferase vector, and IRAK1-expressing vector were transfected in HeLa cells and the luciferase activity was measured by using PicaGene Dual Sea Pansy Luminescence Kit (TOYO B-Net). NF- $\kappa$ B activation was calculated by normalizing Firefly luciferase activity with Renilla luciferase activity.

## Mathematical model

We developed two dynamical models for the inflammation system regulated by Regnase-1 based on different assumptions of the functions of 14-3-3-bound Regnase-1.

### Model 1

In the first model, we assumed that the 14-3-3-bound Regnase-1 does not have the function of degrading its target mRNAs (Figure 4J). The ordinary differential equations are given as follows:

$$\begin{aligned}
 \frac{dx_1}{dt} &= k_1 \text{signal}(t) - d_1 x_1 x_3 - d_4 x_1 \\
 \frac{dx_2}{dt} &= k_2 \text{signal}(t) - d_2 x_2 x_3 - d_5 x_2 \\
 \frac{dx_3}{dt} &= k_3 x_2 - (d_3 + d_6 \text{signal}(t) + d_7 \text{signal}(t)) x_3 + d_9 x_4 \\
 \frac{dx_4}{dt} &= d_7 \text{signal}(t) x_3 - (d_8 + d_9) x_4
 \end{aligned} \tag{1.1}$$

where  $x_1$ ,  $x_2$ ,  $x_3$ , and  $x_4$  is the abundance of *Il6* mRNA, *Zc3h12a* mRNA, Reg1 Protein, and 14-3-3-bound Reg1 Protein, respectively;  $k_1$  and  $k_2$  is the transcription rate constant of *Il6*, and *Zc3h12a*, respectively;  $k_3$  is the translation rate constant of *Zc3h12a*;  $d_1$  and  $d_2$  is

684 the Reg1-induced degradation rate constant of *Il6* mRNA and *Zc3h12a* mRNA, respectively;  
 685  $d_3$ ,  $d_4$ , and  $d_5$  is the Reg1-independent degradation rate constant of Reg1 protein, *Il6*  
 686 mRNA, and *Zc3h12a* mRNA, respectively;  $d_6$  is the ubiquitin-dependent degradation rate  
 687 constant of Reg1 protein;  $d_7$  is the binding rate constant of Reg1 protein to 14-3-3;  $d_8$  is the  
 688 natural degradation rate constant of 14-3-3-bound Reg1 protein;  $d_9$  is the dissociation rate  
 689 constant of Reg1 from 14-3-3.  $signal(t)$  is the strength of TLR stimulation, which is given  
 690 as the following form (Mino et al., 2019):

$$\begin{aligned}
 & signal(t) \\
 & = \begin{cases} s_{base} & (if\ 0 \leq t \leq t_{delay}), \\
 \frac{s_{input} - s_{base}}{t_{raise}}(t - t_{delay}) + s_{base} & (if\ t_{delay} \leq t \leq t_{delay} + t_{raise}), \\
 s_{input} & (if\ t_{delay} + t_{raise} \leq t \leq t_{delay} + t_{raise} + t_{pulse}), \\
 (s_{input} - s_{base}) \times \exp\left(-\frac{t - (t_{delay} + t_{raise} + t_{pulse})}{t_{delay}}\right) + s_{input} & (if\ t > t_{delay} + t_{raise} + t_{pulse}) \end{cases} \quad (1.2)
 \end{aligned}$$

691

## 692 **Model 2**

693 We also developed an alternative model in which the 14-3-3-bound Regnase-1 maintains  
 694 functions of degrading its target mRNAs (Figure 4J). The ordinary differential equations are  
 695 given as follows:

$$\begin{aligned}
\frac{d\hat{x}_1}{dt} &= k_1 \text{signal}(t) - d_1 \hat{x}_1 \hat{x}_3 - d_1' \hat{x}_1 \hat{x}_4 - d_4 \hat{x}_1 \\
\frac{d\hat{x}_2}{dt} &= k_2 \text{signal}(t) - d_2 \hat{x}_2 \hat{x}_3 - d_2' \hat{x}_2 \hat{x}_4 - d_5 \hat{x}_2 \\
\frac{d\hat{x}_3}{dt} &= k_3 x_2 - (d_3 + d_6 \text{signal}(t) + d_7 \text{signal}(t)) \hat{x}_3 + d_9 \hat{x}_4 \\
\frac{d\hat{x}_4}{dt} &= d_7 \text{signal}(t) \hat{x}_3 - (d_8 + d_9) \hat{x}_4
\end{aligned} \tag{1.3}$$

where  $\hat{x}_1$ ,  $\hat{x}_2$ ,  $\hat{x}_3$ , and  $\hat{x}_4$  is the abundance of *Il6* mRNA, *Zc3h12a* mRNA, Reg1 Protein, 14-3-3-bound Reg1 Protein, respectively;  $d_1'$  and  $d_2'$  is the 14-3-3-bound Reg1-induced degradation rate constant of *Il6* mRNA and *Zc3h12a* mRNA, respectively. The other parameters are defined in the same way as Model 1.

To determine which model is consistent with the experimental observations, we focus on the experimental findings that there was no difference in the abundance of *Il6* mRNA, *Zc3h12a* mRNA, and Reg1- protein (without 14-3-3 bound) between *Zc3h12a*<sup>WT/WT</sup> and *Zc3h12a*<sup>S513A/S513A</sup> cells in the late phase of stimulation (Figure 4A, B, D, and E). We will show that in Model 2 (1.3), the abundance of the *Il6* mRNAs should be different between *Zc3h12a*<sup>WT/WT</sup> and *Zc3h12a*<sup>S513A/S513A</sup> cells under the condition that amount of the 14-3-3-free Reg1 protein is comparable between them.

### Analysis of the equilibrium

Lemma 1. For *Zc3h12a*<sup>WT/WT</sup> cells, there exists only one nonnegative (biologically meaningful) equilibrium of the system (1.3) if and only if  $d_3 + d_6 s_{input} + d_7 s_{input} -$

711  $\frac{d_7 d_9 s_{input}}{d_7 s_{input} + d_9} \geq 0$ . If  $d_3 + d_6 s_{input} + d_7 s_{input} - \frac{d_7 d_9 s_{input}}{d_7 s_{input} + d_9} < 0$ , there is no equilibrium. For

712  $Zc3h12a^{S513A/S513A}$  cells, there always exists only one nonnegative (biologically meaningful)  
 713 equilibrium.

714 Proof of lemma 1:

715 Setting all the derivatives of (1.3) equal to zero yields

$$\begin{aligned}
 0 &= k_1 s_{input} - d_1 \hat{X}_1^{WT} \hat{X}_3^{WT} - d_1' \hat{X}_1^{WT} \hat{X}_4^{WT} - d_4 \hat{X}_1^{WT} \\
 0 &= k_2 s_{input} - d_2 \hat{X}_2^{WT} \hat{X}_3^{WT} - d_2' \hat{X}_2^{WT} \hat{X}_4^{WT} - d_5 \hat{X}_2^{WT} \\
 0 &= k_3 \hat{X}_2^{WT} - (d_3 + d_6 s_{input} + d_7 s_{input}) \hat{X}_3^{WT} + d_9 \hat{X}_4^{WT} \\
 0 &= d_7 s_{input} \hat{X}_3^{WT} - (d_8 + d_9) \hat{X}_4^{WT}
 \end{aligned} \tag{1.4}$$

716 where  $\hat{X}_1^{WT}$ ,  $\hat{X}_2^{WT}$ ,  $\hat{X}_3^{WT}$ , and  $\hat{X}_4^{WT}$  are fixed points of  $\hat{x}_1$ ,  $\hat{x}_2$ ,  $\hat{x}_3$ , and  $\hat{x}_4$ , respectively. Given  
 717 that  $signal(t) \rightarrow s_{input}$  as  $t \rightarrow \infty$ , we assume  $signal(t) \approx s_{input}$  at the equilibrium.

718 It follows from (1.4) that

$$\left( d_2 + \frac{d_7 s_{input}}{d_8 + d_9} d_2' \right) K (\hat{X}_3^{WT})^2 + d_5 K \hat{X}_3^{WT} - k_2 s_{input} = 0 \tag{1.5a}$$

719

$$\hat{X}_4^{WT} = \frac{d_7 s_{input}}{d_8 + d_9} \hat{X}_3^{WT} \tag{1.5b}$$

720

$$\hat{X}_2^{WT} = K \hat{X}_3^{WT} \tag{1.5c}$$

721

$$\hat{X}_1^{WT} = \frac{k_1 s_{input}}{d_1 \hat{X}_3^{WT} + d_1' \hat{X}_4^{WT} + d_4} \quad (1.5d)$$

722 where

$$K := \frac{1}{k_3} \left( d_3 + d_6 s_{input} + d_7 s_{input} - \frac{d_7 d_9 s_{input}}{d_7 s_{input} + d_9} \right)$$

723 It is easy to see that the quadratic equation (1.5a) has a nonnegative solution if  $K \geq 0$ , i.e.

724  $d_3 + d_6 s_{input} + d_7 s_{input} - \frac{d_7 d_9 s_{input}}{d_7 s_{input} + d_9} \geq 0$ . If  $K < 0$ , (1.5a) has no nonnegative solution. If

725  $\hat{X}_3^{WT} \geq 0$ , it follows from (1.5b), (1.5c), and (1.5d) that  $\hat{X}_4^{WT}$ ,  $\hat{X}_2^{WT}$ ,  $\hat{X}_1^{WT} \geq 0$ .

726

727 For  $Zc3h12a^{S513A/S513A}$  cells, we assume that  $d_7 = d_8 = d_9 = 0$ . Substituting this

728 equation into (1.4) yields

$$\begin{aligned} 0 &= k_1 s_{input} - d_1 \hat{X}_1^{SA} \hat{X}_3^{SA} - d_4 \hat{X}_1^{SA} \\ 0 &= k_2 s_{input} - d_2 \hat{X}_2^{SA} \hat{X}_3^{SA} - d_5 \hat{X}_2^{SA} \\ 0 &= k_3 \hat{X}_2^{SA} - (d_3 + d_6 s_{input}) \hat{X}_3^{SA} \\ 0 &= \hat{X}_4^{SA} \end{aligned} \quad (1.6)$$

729 where  $\hat{X}_1^{SA}$ ,  $\hat{X}_2^{SA}$ ,  $\hat{X}_3^{SA}$ , and  $\hat{X}_4^{SA}$  are fixed points of  $\hat{x}_1$ ,  $\hat{x}_2$ ,  $\hat{x}_3$ , and  $\hat{x}_4$  in  $Zc3h12a^{S513A/S513A}$

730 cells, respectively.

731 It follows from (1.6) that

$$d_2 \frac{k_3}{d_3 + d_6 s_{input}} (\hat{X}_2^{SA})^2 + d_5 \hat{X}_2^{SA} - k_2 s_{input} = 0 \quad (1.7a)$$

732

$$\hat{X}_3^{SA} = \frac{k_3}{d_3 + d_6 s_{input}} \hat{X}_2^{SA} \quad (1.7b)$$

733

$$\hat{X}_1^{SA} = \frac{k_1 s_{input}}{d_1 \hat{X}_3^{SA} + d_4} \quad (1.7c)$$

734 It is easy to see that the quadratic equation (1.7a) has a nonnegative solution. If  $\hat{X}_2^{SA} \geq 0$ , it  
 735 follows from (1.7b) and (1.7c) that  $\hat{X}_3^{SA} \hat{X}_1^{SA} \geq 0$ .

736

737 Lemma 2. There exists only one nonnegative (biologically meaningful) equilibrium of the  
 738 system (1.1) if and only if  $d_3 + d_6 s_{input} + d_7 s_{input} - \frac{d_7 d_9 s_{input}}{d_7 s_{input} + d_9} \geq 0$ . If  $d_3 + d_6 s_{input} +$   
 739  $d_7 s_{input} - \frac{d_7 d_9 s_{input}}{d_7 s_{input} + d_9} < 0$ , there is no equilibrium. For  $Zc3h12a^{S513A/S513A}$  cells, there

740 always exists only one nonnegative (biologically meaningful) equilibrium.

741 Proof of lemma2:

742 With  $d_1' = d_2' = 0$  in lemma 1, we get the same conclusion.

743

#### 744 Consistency with the experiments

745 The experimental observation shows that there was no difference in the abundance of Reg1  
 746 protein between  $Zc3h12a^{WT/WT}$  and  $Zc3h12a^{S513A/S513A}$  cells at the late phase of stimulation  
 747 (Figure 4A–C), which implies

$$\hat{X}_3^{WT} \approx \hat{X}_3^{SA} \quad (1.8)$$

748 , based on the alternative model (1.3).



749

750 From (1.4) and (1.6), we get

$$\begin{aligned}\hat{X}_1^{WT} &= \frac{k_1 S_{input}}{d_1 \hat{X}_3^{WT} + d_1' \hat{X}_4^{WT} + d_4} \\ \hat{X}_2^{WT} &= \frac{k_2 S_{input}}{d_2 \hat{X}_3^{WT} + d_2' \hat{X}_4^{WT} + d_5}\end{aligned}\tag{1.9a}$$

751

$$\begin{aligned}\hat{X}_1^{SA} &= \frac{k_1 S_{input}}{d_1 \hat{X}_3^{SA} + d_4} \\ \hat{X}_2^{SA} &= \frac{k_2 S_{input}}{d_2 \hat{X}_3^{SA} + d_5}\end{aligned}\tag{1.9b}$$

752 By (1.8), (1.9a), and (1.9b), we obtain

$$\hat{X}_1^{WT} < \hat{X}_1^{SA}\tag{1.10a}$$

753

$$\hat{X}_2^{WT} < \hat{X}_2^{SA}\tag{1.10b}$$

754 (1.10a) and (1.10b) implies that in Model 2, the abundance of *Il6* and *Zc3h12a* mRNA in  
 755 *Zc3h12a*<sup>WT/WT</sup> cells should be smaller than that in *Zc3h12a*<sup>S513A/S513A</sup> cells at the late phase  
 756 under the condition that amount of the Reg1 protein is comparable (1.8) between these two  
 757 cells. It contradicts experimental observation that the abundance of the *Il6* and *Zc3h12a*  
 758 mRNAs did not differ between *Zc3h12a*<sup>WT/WT</sup> and *Zc3h12a*<sup>S513A/S513A</sup> cells (Figure 4D-I).  
 759 Thus, Model 2 (1.3) is not consistent with the experimental findings.

760

In contrast, in Model 1 (1.1), we assume from experimental findings that

$$X_3^{WT} \approx X_3^{SA} \quad (1.11)$$

761 , just like (1.8), where  $X_3^{WT}$  is the fixed point of  $x_3$  in  $Zc3h12a^{WT/WT}$  cells and  $X_3^{SA}$  is the  
 762 fixed point of  $x_3$  in  $Zc3h12a^{S513A/S513A}$  cells based on the model (1.1).

763 By substituting  $d_7 = d_8 = d_9 = 0$  into (1.9a) and (1.9b), we obtain

$$\begin{aligned} X_1^{WT} &= \frac{k_1 S_{input}}{d_1 X_3^{WT} + d_4} \\ X_2^{WT} &= \frac{k_2 S_{input}}{d_2 X_3^{WT} + d_5} \end{aligned} \quad (1.12a)$$

764

$$\begin{aligned} X_1^{SA} &= \frac{k_1 S_{input}}{d_1 X_3^{SA} + d_4} \\ X_2^{SA} &= \frac{k_2 S_{input}}{d_2 X_3^{SA} + d_5} \end{aligned} \quad (1.12b)$$

765 where  $X_1^{WT}$  and  $X_2^{WT}$  are fixed points of  $x_1$  and  $x_2$ , respectively in  $Zc3h12a^{WT/WT}$  cells and

766  $X_1^{SA}$  and  $X_2^{SA}$  are fixed points of  $x_1$  and  $x_2$ , respectively in  $Zc3h12a^{S513A/S513A}$  cells.

767 By (1.11), (1.12a), and (1.12b), we obtain

$$X_1^{WT} \approx X_1^{SA} \quad (1.13a)$$

768

$$X_2^{WT} \approx X_2^{SA} \quad (1.13b)$$

769 In this case, (1.13a) and (1.13b) are in agreement with the experimental facts that that the

770 abundance of the target mRNAs did not differ between  $Zc3h12a^{WT/WT}$  and  $Zc3h12a^{S513A/S513A}$

771 cells.

772 These mathematical analyses indicate that Model 1 (1.1), but not Model 2 (1.3), is

consistent with the experimental findings.

### **Immunofluorescence**

Cells were cultured on cover glass, fixed with 4%-Paraformaldehyde Phosphate Buffer Solution (nacalai tesque), and permeabilized with 0.5 % (vol/vol) Triton X-100 (nacalai tesque) in PBS, followed by incubation in blocking solution (2 % (vol/vol) goat serum (FUJIFILM Wako Pure Chemical) and 0.1 % (wt/vol) gelatin in PBS). The antibodies used in Immunofluorescence were listed in the key resources table. DNA was stained with Hoechst 33342 (Invitrogen). Fluorescence was detected with TCS SPE (Leica). Acquired images were analyzed with Fiji (Schindelin et al., 2012).

### **Amino acid sequence analysis**

Amino acid sequence of each protein was obtained from NCBI. The results of T-coffee alignment (Notredame et al., 2000) were visualized by using Jalview (Waterhouse et al., 2009). Secondary structure was predicted by using PSIPRED 4.0 (Buchan & Jones, 1999; Jones, 1999). NES prediction was performed by using LocNES (Xu et al., 2015).

### **Data availability**

Mass spectrometry data have been deposited to the ProteomeXchange Consortium (<http://proteomecentral.proteomexchange.org>) via the jPOST partner repository (Moriya et al., 2019; Okuda et al., 2017) (<http://jpostdb.org>) with the data set identifier PXD026561.

RNA sequencing data have been deposited to GEO (Accession code: GSE180028).

**Acknowledgements**

We thank S. Ogawa and N. Kakiuchi in Kyoto university for performing RNA sequencing and providing *ZC3H12A*-KO HeLa cells, Y. Okumoto for secretarial assistance and lab members for helpful discussion. This work was supported by Japan Society for the Promotion of Science (JSPS) KAKENHI [18H05278]; AMED-FORCE [JP20gm4010002] from Japan Agency for Medical Research and Development and the JSPS through Core-to-Core Program. K.A. was supported by “Kibou Projects” Scholarship for doctoral Students in Immunology. T.M. was funded by JSPS KAKENHI (19H03488), Grant-in-Aid for Scientific Research on Innovative Areas “Genome Science” (221S0002 and 16H06279), Takeda Science Foundation, the Uehara Memorial Foundation, Shimizu Foundation for Immunology and Neuroscience, Naito Foundation, Senri Life Science Foundation, Nakajima Foundation, and Mochida Memorial Foundation for Medical and Pharmaceutical Research.

## References

- Afgan, E., Baker, D., Batut, B., Van Den Beek, M., Bouvier, D., Ech, M., Chilton, J., Clements, D., Coraor, N., Grüning, B. A., Guerler, A., Hillman-Jackson, J., Hiltemann, S., Jalili, V., Rasche, H., Soranzo, N., Goecks, J., Taylor, J., Nekrutenko, A., & Blankenberg, D. (2018). The Galaxy platform for accessible, reproducible and collaborative biomedical analyses: 2018 update. *Nucleic Acids Research*, 46(W1), W537–W544. <https://doi.org/10.1093/nar/gky379>
- Aitken, A. (2006). 14-3-3 proteins: A historic overview. *Seminars in Cancer Biology*, 16(3), 162–172. <https://doi.org/10.1016/j.semcancer.2006.03.005>
- Akira, S., Uematsu, S., & Takeuchi, O. (2006). Pathogen recognition and innate immunity. *Cell*, 124(4), 783–801. <https://doi.org/10.1016/j.cell.2006.02.015>
- Anderson, P. (2010). Post-transcriptional regulons coordinate the initiation and resolution of inflammation. *Nature Reviews Immunology*, 10(1), 24–35. <https://doi.org/10.1038/nri2685>
- Buchan, D. W. A., & Jones, D. T. (2019). The PSIPRED Protein Analysis Workbench: 20 years on. *Nucleic Acids Research*, 47(W1), W402–W407. <https://doi.org/10.1093/nar/gkz297>
- Carpenter, S., Ricci, E. P., Mercier, B. C., Moore, M. J., & Fitzgerald, K. A. (2014). Post-transcriptional regulation of gene expression in innate immunity. *Nature Reviews Immunology*, 14(6), 361–376. <https://doi.org/10.1038/nri3682>
- Cong, L., Ran, F. A., Cox, D., Lin, S., Barretto, R., Habib, N., Hsu, P. D., Wu, X., Jiang, W.,

- 827       Marraffini, L. A., & Zhang, F. (2013). Multiplex genome engineering using  
828       CRISPR/Cas systems. *Science*, 339(6121), 819–823.  
829       <https://doi.org/10.1126/science.1231143>
- 830       Dau, T., Bartolomucci, G., & Rappsilber, J. (2020). Proteomics Using Protease Alternatives  
831       to Trypsin Benefits from Sequential Digestion with Trypsin. *Analytical Chemistry*,  
832       92(14), 9523–9527. <https://doi.org/10.1021/acs.analchem.0c00478>
- 833       Davis, M., Hatzubai, A., Andersen, J. S., Ben-Shushan, E., Fisher, G. Z., Yaron, A., Bauskin,  
834       A., Mercurio, F., Mann, M., & Ben-Neriah, Y. (2002). Pseudosubstrate regulation of the  
835       SCF $\beta$ -TrCP ubiquitin ligase by hnRNP-U. *Genes and Development*, 16(4), 439–451.  
836       <https://doi.org/10.1101/gad.218702>
- 837       Fitzgerald, K. A., & Kagan, J. C. (2020). Toll-like Receptors and the Control of Immunity.  
838       *Cell*, 180(6), 1044–1066. <https://doi.org/10.1016/j.cell.2020.02.041>
- 839       Flannery, S. M., Keating, S. E., Szymak, J., & Bowie, A. G. (2011). Human interleukin-1  
840       receptor-associated kinase-2 is essential for toll-like receptor-mediated transcriptional  
841       and post-transcriptional regulation of tumor necrosis factor  $\alpha$ . *Journal of Biological*  
842       *Chemistry*, 286(27), 23688–23697. <https://doi.org/10.1074/jbc.M111.248351>
- 843       Fu, H., Coburn, J., & Collier, R. J. (1993). The eukaryotic host factor that activates  
844       exoenzyme S of *Pseudomonas aeruginosa* is a member of the 14-3-3 protein family.  
845       *Proceedings of the National Academy of Sciences of the United States of America*, 90(6),  
846       2320–2324. <https://doi.org/10.1073/pnas.90.6.2320>
- 847       Fujihara, Y., & Ikawa, M. (2014). CRISPR/Cas9-based genome editing in mice by single

- 848 plasmid injection. In *Methods in Enzymology* (Vol. 546, Issue C, pp. 319–336).  
 849 Academic Press Inc. <https://doi.org/10.1016/B978-0-12-801185-0.00015-5>
- 850 Gottipati, S., Rao, N. L., & Fung-Leung, W. P. (2008). IRAK1: A critical signaling mediator  
 851 of innate immunity. *Cellular Signalling*, 20(2), 269–276.  
 852 <https://doi.org/10.1016/j.cellsig.2007.08.009>
- 853 Guo, C. J., Ma, X. K., Xing, Y. H., Zheng, C. C., Xu, Y. F., Shan, L., Zhang, J., Wang, S.,  
 854 Wang, Y., Carmichael, G. G., Yang, L., & Chen, L. L. (2020). Distinct Processing of  
 855 lncRNAs Contributes to Non-conserved Functions in Stem Cells. *Cell*, 181(3),  
 856 621–636.e22. <https://doi.org/10.1016/j.cell.2020.03.006>
- 857 Hao, S., & Baltimore, D. (2009). The stability of mRNA influences the temporal order of the  
 858 induction of genes encoding inflammatory molecules. *Nature Immunology*, 10(3), 281–  
 859 288. <https://doi.org/10.1038/ni.1699>
- 860 Hartupée, J., Li, X., & Hamilton, T. (2008). Interleukin 1 $\alpha$ -induced NF $\kappa$ B activation and  
 861 chemokine mRNA stabilization diverge at IRAK. *Journal of Biological Chemistry*,  
 862 283(23), 15689–15693. <https://doi.org/10.1074/jbc.M801346200>
- 863 Hutten, S., & Kehlenbach, R. H. (2007). CRM1-mediated nuclear export: to the pore and  
 864 beyond. *Trends in Cell Biology*, 17(4), 193–201.  
 865 <https://doi.org/10.1016/j.tcb.2007.02.003>
- 866 Iwasaki, H., Takeuchi, O., Teraguchi, S., Matsushita, K., Uehata, T., Kuniyoshi, K., Satoh, T.,  
 867 Saitoh, T., Matsushita, M., Standley, D. M., & Akira, S. (2011). The I $\kappa$ B kinase  
 868 complex regulates the stability of cytokine-encoding mRNA induced by TLR–IL-1R by

- 869 controlling degradation of regnase-1. *Nature Immunology*, 12(12), 1167–1175.  
870 <https://doi.org/10.1038/ni.2137>
- 871 Jones, D. T. (1999). Protein secondary structure prediction based on position-specific scoring  
872 matrices. *Journal of Molecular Biology*, 292(2), 195–202.  
873 <https://doi.org/10.1006/jmbi.1999.3091>
- 874 Kakiuchi, N., Yoshida, K., Uchino, M., Kihara, T., Akaki, K., Inoue, Y., Kawada, K.,  
875 Nagayama, S., Yokoyama, A., Yamamoto, S., Matsuura, M., Horimatsu, T., Hirano, T.,  
876 Goto, N., Takeuchi, Y., Ochi, Y., Shiozawa, Y., Kogure, Y., Watatani, Y., ... Ogawa, S.  
877 (2020). Frequent mutations that converge on the NFKBIZ pathway in ulcerative colitis.  
878 *Nature*, 577(7789), 260–265. <https://doi.org/10.1038/s41586-019-1856-1>
- 879 Karlberg, T., Hornyak, P., Pinto, A. F., Milanova, S., Ebrahimi, M., Lindberg, M., Püllen, N.,  
880 Nordström, A., Löverli, E., Caraballo, R., Wong, E. V., Näreoja, K., Thorsell, A. G.,  
881 Elofsson, M., De La Cruz, E. M., Björkegren, C., & Schüler, H. (2018). 14-3-3 proteins  
882 activate Pseudomonas exotoxins-S and -T by chaperoning a hydrophobic surface.  
883 *Nature Communications*, 9(1), 1–11. <https://doi.org/10.1038/s41467-018-06194-1>
- 884 Kollewe, C., Mackensen, A. C., Neumann, D., Knop, J., Cao, P., Li, S., Wesche, H., &  
885 Martin, M. U. (2004). Sequential Autophosphorylation Steps in the Interleukin-1  
886 Receptor-associated Kinase-1 Regulate its Availability as an Adapter in Interleukin-1  
887 Signaling. *Journal of Biological Chemistry*, 279(7), 5227–5236.  
888 <https://doi.org/10.1074/jbc.M309251200>
- 889 la Cour, T., Gupta, R., Rapacki, K., Skriver, K., Poulsen, F. M., & Brunak, S. (2003).



890 NESbase version 1.0: A database of nuclear export signals. *Nucleic Acids Research*,  
891 31(1), 393–396. <https://doi.org/10.1093/nar/gkg101>

892 MacLean, B., Tomazela, D. M., Shulman, N., Chambers, M., Finney, G. L., Frewen, B., Kern,  
893 R., Tabb, D. L., Liebler, D. C., & MacCoss, M. J. (2010). Skyline: An open source  
894 document editor for creating and analyzing targeted proteomics experiments.  
895 *Bioinformatics*, 26(7), 966–968. <https://doi.org/10.1093/bioinformatics/btq054>

896 Maquat, L. E., Tarn, W. Y., & Isken, O. (2010). The pioneer round of translation: Features  
897 and functions. *Cell*, 142(3), 368–374. <https://doi.org/10.1016/j.cell.2010.07.022>

898 Masters, S. C., Pederson, K. J., Zhang, L., Barbieri, J. T., & Fu, H. (1999). Interaction of  
899 14-3-3 with a nonphosphorylated protein ligand, exoenzyme S of *Pseudomonas*  
900 *aeruginosa*. *Biochemistry*, 38(16), 5216–5221. <https://doi.org/10.1021/bi982492m>

901 Matsushita, K., Takeuchi, O., Standley, D. M., Kumagai, Y., Kawagoe, T., Miyake, T., Satoh,  
902 T., Kato, H., Tsujimura, T., Nakamura, H., & Akira, S. (2009). Zc3h12a is an RNase  
903 essential for controlling immune responses by regulating mRNA decay. *Nature*,  
904 458(7242), 1185–1190. <https://doi.org/10.1038/nature07924>

905 Meerbrey, K. L., Hu, G., Kessler, J. D., Roarty, K., Li, M. Z., Fang, J. E., Herschkowitz, J. I.,  
906 Burrows, A. E., Ciccio, A., Sun, T., Schmitt, E. M., Bernardi, R. J., Fu, X., Bland, C. S.,  
907 Cooper, T. A., Schiff, R., Rosen, J. M., Westbrook, T. F., & Elledge, S. J. (2011). The  
908 pINDUCER lentiviral toolkit for inducible RNA interference in vitro and in vivo.  
909 *Proceedings of the National Academy of Sciences of the United States of America*,  
910 108(9), 3665–3670. <https://doi.org/10.1073/pnas.1019736108>

- 911 Mino, T., Iwai, N., Endo, M., Inoue, K., Akaki, K., Hia, F., Uehata, T., Emura, T., Hidaka, K.,  
 912 Suzuki, Y., Standley, D. M., Okada-Hatakeyama, M., Ohno, S., Sugiyama, H.,  
 913 Yamashita, A., & Takeuchi, O. (2019). Translation-dependent unwinding of stem–  
 914 loops by UPF1 licenses Regnase-1 to degrade inflammatory mRNAs. *Nucleic Acids*  
 915 *Research*. <https://doi.org/10.1093/nar/gkz628>
- 916 Mino, T., Murakawa, Y., Fukao, A., Vandenbon, A., Wessels, H. H., Ori, D., Uehata, T.,  
 917 Tartey, S., Akira, S., Suzuki, Y., Vinuesa, C. G., Ohler, U., Standley, D. M., Landthaler,  
 918 M., Fujiwara, T., & Takeuchi, O. (2015). Regnase-1 and roquin regulate a common  
 919 element in inflammatory mRNAs by spatiotemporally distinct mechanisms. *Cell*,  
 920 *161*(5), 1058–1073. <https://doi.org/10.1016/j.cell.2015.04.029>
- 921 Moriya, Y., Kawano, S., Okuda, S., Watanabe, Y., Matsumoto, M., Takami, T., Kobayashi,  
 922 D., Yamanouchi, Y., Araki, N., Yoshizawa, A. C., Tabata, T., Iwasaki, M., Sugiyama,  
 923 N., Tanaka, S., Goto, S., & Ishihama, Y. (2019). The jpost environment: An integrated  
 924 proteomics data repository and database. *Nucleic Acids Research*, *47*(D1), D1218–  
 925 D1224. <https://doi.org/10.1093/nar/gky899>
- 926 Müller-Mcnicoll, M., & Neugebauer, K. M. (2013). How cells get the message: Dynamic  
 927 assembly and function of mRNA-protein complexes. *Nature Reviews Genetics*, *14*(4),  
 928 275–287. <https://doi.org/10.1038/nrg3434>
- 929 Muslin, A. J., Tanner, J. W., Allen, P. M., & Shaw, A. S. (1996). Interaction of 14-3-3 with  
 930 signaling proteins is mediated by the recognition of phosphoserine. *Cell*, *84*(6), 889–  
 931 897. [https://doi.org/10.1016/S0092-8674\(00\)81067-3](https://doi.org/10.1016/S0092-8674(00)81067-3)

- 932 Nakagami, H., Sugiyama, N., Mochida, K., Daudi, A., Yoshida, Y., Toyoda, T., Tomita, M.,  
933 Ishihama, Y., & Shirasu, K. (2010). Large-scale comparative phosphoproteomics  
934 identifies conserved phosphorylation sites in plants. *Plant Physiology*, 153(3), 1161–  
935 1174. <https://doi.org/10.1104/pp.110.157347>
- 936 Nanki, K., Fujii, M., Shimokawa, M., Matano, M., Nishikori, S., Date, S., Takano, A.,  
937 Toshimitsu, K., Ohta, Y., Takahashi, S., Sugimoto, S., Ishimaru, K., Kawasaki, K.,  
938 Nagai, Y., Ishii, R., Yoshida, K., Sasaki, N., Hibi, T., Ishihara, S., ... Sato, T. (2020).  
939 Somatic inflammatory gene mutations in human ulcerative colitis epithelium. 254 /  
940 *Nature* , 577. <https://doi.org/10.1038/s41586-019-1844-5>
- 941 Neidel, S., Ren, H., Torres, A. A., & Smith, G. L. (2019). NF-κB activation is a turn on for  
942 vaccinia virus phosphoprotein A49 to turn off NF-κB activation. *Proceedings of the*  
943 *National Academy of Sciences of the United States of America*, 116(12), 5699–5704.  
944 <https://doi.org/10.1073/pnas.1813504116>
- 945 Notredame, C., Higgins, D. G., & Heringa, J. (2000). T-coffee: A novel method for fast and  
946 accurate multiple sequence alignment. *Journal of Molecular Biology*, 302(1), 205–217.  
947 <https://doi.org/10.1006/jmbi.2000.4042>
- 948 O'Neill, L. A. J., Golenbock, D., & Bowie, A. G. (2013). The history of Toll-like  
949 receptors-redefining innate immunity. *Nature Reviews Immunology*, 13(6), 453–460.  
950 <https://doi.org/10.1038/nri3446>
- 951 Okuda, S., Watanabe, Y., Moriya, Y., Kawano, S., Yamamoto, T., Matsumoto, M., Takami,  
952 T., Kobayashi, D., Araki, N., Yoshizawa, A. C., Tabata, T., Sugiyama, N., Goto, S., &

- 953 Ishihama, Y. (2017). JPOSTrepo: An international standard data repository for  
954 proteomes. *Nucleic Acids Research*, 45(D1), D1107–D1111.  
955 <https://doi.org/10.1093/nar/gkw1080>
- 956 Ottmann, C., Yasmin, L., Weyand, M., Veesenmeyer, J. L., Diaz, M. H., Palmer, R. H.,  
957 Francis, M. S., Hauser, A. R., Wittinghofer, A., & Hallberg, B. (2007).  
958 Phosphorylation-independent interaction between 14-3-3 and exoenzyme S: From  
959 structure to pathogenesis. *EMBO Journal*, 26(3), 902–913.  
960 <https://doi.org/10.1038/sj.emboj.7601530>
- 961 Pennington, K. L., Chan, T. Y., Torres, • Mp, & Andersen, • Jl. (2018). The dynamic and  
962 stress-adaptive signaling hub of 14-3-3: emerging mechanisms of regulation and  
963 context-dependent protein-protein interactions. *Oncogene*, 37, 5587–5604.  
964 <https://doi.org/10.1038/s41388-018-0348-3>
- 965 Rappsilber, J., Mann, M., & Ishihama, Y. (2007). Protocol for micro-purification,  
966 enrichment, pre-fractionation and storage of peptides for proteomics using StageTips.  
967 *Nature Protocols*, 2(8), 1896–1906. <https://doi.org/10.1038/nprot.2007.261>
- 968 Schindelin, J., Arganda-Carreras, I., Frise, E., Kaynig, V., Longair, M., Pietzsch, T.,  
969 Preibisch, S., Rueden, C., Saalfeld, S., Schmid, B., Tinevez, J. Y., White, D. J.,  
970 Hartenstein, V., Eliceiri, K., Tomancak, P., & Cardona, A. (2012). Fiji: An open-source  
971 platform for biological-image analysis. *Nature Methods*, 9(7), 676–682.  
972 <https://doi.org/10.1038/nmeth.2019>
- 973 Shannon, P., Markiel, A., Ozier, O., Baliga, N. S., Wang, J. T., Ramage, D., Amin, N.,

- 974 Schwikowski, B., & Ideker, T. (2003). Cytoscape: A software Environment for  
975 integrated models of biomolecular interaction networks. *Genome Research*, 13(11),  
976 2498–2504. <https://doi.org/10.1101/gr.1239303>
- 977 Sugiyama, N., Imamura, H., & Ishihama, Y. (2019). Large-scale Discovery of Substrates of  
978 the Human Kinome. *Scientific Reports* 2019 9:1, 9(1), 1–12.  
979 <https://doi.org/10.1038/s41598-019-46385-4>
- 980 Szklarczyk, D., Gable, A. L., Lyon, D., Junge, A., Wyder, S., Huerta-Cepas, J., Simonovic,  
981 M., Doncheva, N. T., Morris, J. H., Bork, P., Jensen, L. J., & Von Mering, C. (2019).  
982 STRING v11: Protein-protein association networks with increased coverage,  
983 supporting functional discovery in genome-wide experimental datasets. *Nucleic Acids*  
984 *Research*, 47(D1), D607–D613. <https://doi.org/10.1093/nar/gky1131>
- 985 Takeuchi, O., & Akira, S. (2010). Pattern Recognition Receptors and Inflammation. *Cell*,  
986 140(6), 805–820. <https://doi.org/10.1016/j.cell.2010.01.022>
- 987 Tanaka, H., Arima, Y., Kamimura, D., Tanaka, Y., Takahashi, N., Uehata, T., Maeda, K.,  
988 Satoh, T., Murakami, M., & Akira, S. (2019). Phosphorylation-dependent Regnase-1  
989 release from endoplasmic reticulum is critical in IL-17 response. *Journal of*  
990 *Experimental Medicine*, 216(6). <https://doi.org/10.1084/jem.20181078>
- 991 Turner, M., & Díaz-Muñoz, M. D. (2018). RNA-binding proteins control gene expression  
992 and cell fate in the immune system review-article. In *Nature Immunology* (Vol. 19,  
993 Issue 2, pp. 120–129). Nature Publishing Group.  
994 <https://doi.org/10.1038/s41590-017-0028-4>

- 995 Uehata, T., Iwasaki, H., Vandenbon, A., Matsushita, K., Hernandez-Cuellar, E., Kuniyoshi,  
996 K., Satoh, T., Mino, T., Suzuki, Y., Standley, D. M., Tsujimura, T., Rakugi, H., Isaka,  
997 Y., Takeuchi, O., & Akira, S. (2013). Malt1-induced cleavage of regnase-1 in CD4(+)   
998 helper T cells regulates immune activation. *Cell*, 153(5), 1036–1049.  
999 <https://doi.org/10.1016/j.cell.2013.04.034>
- 1000 van Buuren, N., Burles, K., Schriewer, J., Mehta, N., Parker, S., Buller, R. M., & Barry, M.  
1001 (2014). EVM005: An Ectromelia-Encoded Protein with Dual Roles in NF-κB Inhibition  
1002 and Virulence. *PLoS Pathogens*, 10(8), 1004326.  
1003 <https://doi.org/10.1371/journal.ppat.1004326>
- 1004 Verdoodt, B., Benzinger, A., Popowicz, G. M., Holak, T. A., & Hermeking, H. (2006).  
1005 Characterization of 14-3-3sigma dimerization determinants: Requirement of  
1006 homodimerization for inhibition of cell proliferation. *Cell Cycle*, 5(24), 2920–2926.  
1007 <https://doi.org/10.4161/cc.5.24.3571>
- 1008 Wan, Y., Xiao, H., Affolter, J., Kim, T. W., Bulek, K., Chaudhuri, S., Carlson, D., Hamilton,  
1009 T., Mazumder, B., Stark, G. R., Thomas, J., & Li, X. (2009). Interleukin-1  
1010 receptor-associated kinase 2 is critical for lipopolysaccharide-mediated  
1011 post-transcriptional control. *Journal of Biological Chemistry*, 284(16), 10367–10375.  
1012 <https://doi.org/10.1074/jbc.M807822200>
- 1013 Waterhouse, A. M., Procter, J. B., Martin, D. M. A., Clamp, M., & Barton, G. J. (2009).  
1014 Jalview Version 2-A multiple sequence alignment editor and analysis workbench.  
1015 *Bioinformatics*, 25(9), 1189–1191. <https://doi.org/10.1093/bioinformatics/btp033>

- 1016 Wei, J., Long, L., Zheng, W., Dhungana, Y., Lim, S. A., Guy, C., Wang, Y., Wang, Y. D.,  
1017 Qian, C., Xu, B., Kc, A., Saravia, J., Huang, H., Yu, J., Doench, J. G., Geiger, T. L., &  
1018 Chi, H. (2019). Targeting REGNASE-1 programs long-lived effector T cells for cancer  
1019 therapy. *Nature*, 576(7787), 471–476. <https://doi.org/10.1038/s41586-019-1821-z>  
1020 Wesche, H., Henzel, W. J., Shillinglaw, W., Li, S., & Cao, Z. (1997). MyD88: An adapter  
1021 that recruits IRAK to the IL-1 receptor complex. *Immunity*, 7(6), 837–847.  
1022 [https://doi.org/10.1016/S1074-7613\(00\)80402-1](https://doi.org/10.1016/S1074-7613(00)80402-1)  
1023 Xu, D., Marquis, K., Pei, J., Fu, S. C., Calatay, T., Grishin, N. V., & Chook, Y. M. (2015).  
1024 LocNES: A computational tool for locating classical NESs in CRM1 cargo proteins.  
1025 *Bioinformatics*, 31(9), 1357–1365. <https://doi.org/10.1093/bioinformatics/btu826>  
1026 Yaffe, M. B., Rittinger, K., Volinia, S., Caron, P. R., Aitken, A., Leffers, H., Gambin, S. J.,  
1027 Smerdon, S. J., & Cantley, L. C. (1997). The structural basis for 14-3-3:phosphopeptide  
1028 binding specificity. *Cell*, 91(7), 961–971.  
1029 [https://doi.org/10.1016/S0092-8674\(00\)80487-0](https://doi.org/10.1016/S0092-8674(00)80487-0)  
1030 Yang, Q., Li, K., Huang, X., Zhao, C., Mei, Y., Li, X., Jiao, L., & Yang, H. (2020). lncRNA  
1031 SLC7A11-AS1 Promotes Chemoresistance by Blocking SCF $\beta$ -TRCP-Mediated  
1032 Degradation of NRF2 in Pancreatic Cancer. *Molecular Therapy - Nucleic Acids*, 19,  
1033 974–985. <https://doi.org/10.1016/j.omtn.2019.11.035>  
1034 Yashiroda, Y., & Yoshida, M. (2005). Nucleo-Cytoplasmic Transport of Proteins as a Target  
1035 for Therapeutic Drugs. *Current Medicinal Chemistry*, 10(9), 741–748.  
1036 <https://doi.org/10.2174/0929867033457791>

- 1037 Yasmin, L., Jansson, A. L., Panahandeh, T., Palmer, R. H., Francis, M. S., & Hallberg, B.  
1038 (2006). Delineation of exoenzyme S residues that mediate the interaction with 14-3-3  
1039 and its biological activity. *FEBS Journal*, 273(3), 638–646.  
1040 <https://doi.org/10.1111/j.1742-4658.2005.05100.x>
- 1041 Ye, H., Arron, J. R., Lamothe, B., Cirilli, M., Kobayashi, T., Shevde, N. K., Segal, D.,  
1042 Dzivenu, O. K., Vologodskaya, M., Yim, M., Du, K., Singh, S., Pike, J. W., Darnay, B.  
1043 G., Choi, Y., & Wu, H. (2002). Distinct molecular mechanism for initiating TRAF6  
1044 signalling. *Nature*, 418(6896), 443–447. <https://doi.org/10.1038/nature00888>
- 1045 Yokogawa, M., Tsushima, T., Noda, N. N., Kumeta, H., Enokizono, Y., Yamashita, K.,  
1046 Standley, D. M., Takeuchi, O., Akira, S., & Inagaki, F. (2016). Structural basis for the  
1047 regulation of enzymatic activity of Regnase-1 by domain-domain interactions. *Scientific*  
1048 *Reports*, 6, 22324. <https://doi.org/10.1038/srep22324>



## Figure Legends

### Figure 1

IL-1 $\beta$  or TLR1/2/4/7/8/9-ligand stimulation induces Regnase-1-14-3-3 interaction.

(A) Schematic illustration of the DSP-crosslinking workflow. (B) Protein-protein interaction of the Regnase-1 (Reg1)-associating proteins. Each node represents Regnase-1 associating protein. The proteins whose association with Regnase-1 is weakened or enhanced in IL-1 $\beta$ -stimulated cells are colored in blue or red, respectively. (C) Immunoblot analysis of immunoprecipitates (IP: Myc or IP: HA) and WCL (whole cell lysates) from HeLa cells transiently expressing Myc-14-3-3 $\epsilon$  and HA- $\beta$ TRCP1 stimulated with IL-1 $\beta$  (10 ng/ml) for indicated time. (D) Immunoblot analysis of immunoprecipitates (IP: Myc) and WCL from RAW264.7 or RAW264.7 stably expressing Myc-14-3-3 $\epsilon$  stimulated with Pam<sub>3</sub>CSK<sub>4</sub> (10 ng/ml), poly I:C (100  $\mu$ g/ml), LPS (100 ng/ml), R848 (100 nM), or CpG DNA (1  $\mu$ M) for 4 hours.

### Figure 2

IL-1 $\beta$ -induced phosphorylation of Regnase-1 at S494 and S513 is necessary for Regnase-1-14-3-3 binding.

(A) Immunoblot analysis of  $\lambda$ PP-treated immunoprecipitates (IP: HA) and WCL from HeLa cells transiently expressing HA-14-3-3 $\epsilon$  stimulated with IL-1 $\beta$  (10 ng/ml) for 4 hours. S.E.: short exposure, L.E.: long exposure. (B) The intensity of Regnase-1-bands in (A). (C) Quantitation of phosphosites on Regnase-1 in HeLa cells stimulated with or without IL-1 $\beta$  (10 ng/ml) for 4 hours. Each dot shows phosphosite quantitative ratio between IL-1 $\beta$  + and IL-1 $\beta$  -. Phosphosites with log<sub>2</sub> ratio > 1 were colored with red. Black horizontal line shows Regnase-1 protein quantitative ratio derived from the average of non-phosphopeptide quantitative ratios, and its error bars show the standard deviation. (D) Immunoblot analysis

of immunoprecipitates (IP: HA) and WCL from HeLa cells transiently expressing HA-14-3-3 $\epsilon$  and FLAG-Regnase-1-WT or indicated mutants stimulated with IL-1 $\beta$  (10 ng/ml) for 4 hours. (E) Schematic illustration of Regnase-1 protein. The amino acid sequence including S494 and S513 shown in (F) is highlighted in green. NTD: N-terminal domain, ZF: Zinc finger domain, CTD: C-terminal domain. (F) The amino acid sequences including S494 and S513 of Regnase-1 from mouse and other indicated vertebrates. (G) Immunoblot analysis of immunoprecipitates (IP: Myc) and WCL from HeLa cells transiently expressing Myc-14-3-3 $\epsilon$ , HA-IRAK1/2, and FLAG-Regnase-1-WT or indicated mutants. (H) Schematic illustration of IRAK1 protein. The amino acid sequence in CSD of IRAK1 and IRAK2 from mouse and other indicated vertebrates are also shown. DD: Death domain, CSD: C-terminal structural domain. (I) Immunoblot analysis of immunoprecipitates (IP: HA) and WCL from HeLa cells transiently expressing FLAG-Regnase-1-WT, HA-14-3-3 $\epsilon$ , and Myc-IRAK1-WT or indicated mutants.

### Figure 3

$\beta$ TRCP binds to 14-3-3-free Regnase-1.

(A) Immunoblot analysis of immunoprecipitates (IP: Myc) and WCL from HeLa cells transiently expressing Myc-14-3-3 $\epsilon$  and HA-Regnase-1-WT or indicated mutants stimulated with IL-1 $\beta$  (10 ng/ml) for 4 hours. (B) Immunoblot analysis of immunoprecipitates (IP: FLAG) and WCL from HeLa cells transiently expressing FLAG- $\beta$ TRCP1 and HA-Regnase-1-WT or indicated mutants stimulated with IL-1 $\beta$  (10 ng/ml) for 4 hours. (C) Immunoblot analysis of immunoprecipitates (IP: FLAG or HA) and WCL from HeLa cells transiently expressing FLAG- $\beta$ TRCP- $\Delta$ F and HA-14-3-3 $\epsilon$  stimulated with IL-1 $\beta$  (10 ng/ml) for 4 hours. S.E.: short exposure, L.E.: long exposure. (D) The intensity of Regnase-1-bands in (C).

**Figure 4**

The S513A mutation destabilizes Regnase-1 protein but does not affect target mRNA abundance.

(A)-(C) Immunoblot analysis of *Zc3h12a*<sup>WT/WT</sup> and *Zc3h12a*<sup>S513A/S513A</sup> MEFs stimulated with IL-1 $\beta$  (10 ng/ml) (A), BMDMs stimulated with LPS (100 ng/ml) (B), and thioglycollate-elicited PECs stimulated with LPS (100 ng/ml) (C) for indicated time. PECs were pretreated with MG-132 (5  $\mu$ M) 2 hours before the stimulation. (D)-(F) mRNA expression of *Zc3h12a* and *Il6* in *Zc3h12a*<sup>WT/WT</sup> and *Zc3h12a*<sup>S513A/S513A</sup> MEFs stimulated with IL-1 $\beta$  (10 ng/ml) for 4 hours (D), BMDMs stimulated with LPS (100 ng/ml) for 4 hours (E), and thioglycollate-elicited PECs stimulated with LPS (100 ng/ml) for indicated time (F). (G)-(I) IL-6 secretion in *Zc3h12a*<sup>WT/WT</sup> and *Zc3h12a*<sup>S513A/S513A</sup> MEFs stimulated with IL-1 $\beta$  (10 ng/ml), IL-17A (50 ng/ml), or TNF (10 ng/ml) for 24 hours (G), BMDMs stimulated with Pam<sub>3</sub>CSK<sub>4</sub> (1 or 10 ng/ml), poly I:C (10 or 100  $\mu$ g/ml), LPS (10 or 100 ng/ml), R848 (10 or 100 nM), or CpG DNA (0.1 or 1  $\mu$ M) for 24 hours (H), and thioglycollate-elicited PECs stimulated with LPS (100 ng/ml), R848 (100 nM), or IL-1 $\beta$  (10 ng/ml) for 24 hours (I). (J) Schematic representation of Model 1 in which 14-3-3-bound Regnase-1 does not have the function of degrading its target mRNAs. This model could explain the experimental observations. (K) Schematic representation of Model 2 in which 14-3-3-bound Regnase-1 maintains some ability to degrade its target mRNAs. This model is not consistent with the experimental observations.

In (D)-(I), bars represent mean values of biological replicates ( $n = 3$ ), and error bars represent standard deviation. Data is representative of two independent experiments, each with three biological replicates.

**Figure 5**

14-3-3 bound to phospho-S494 and S513 inactivates Regnase-1 by inhibiting Regnase-1-mRNA binding.

(A) Immunoblot analysis of ZC3H12A-KO HeLa cells transiently expressing Regnase-1-WT or indicated mutants. Cells were stimulated with IL-1 $\beta$  (10 ng/ml) for indicated time. (B) mRNA expression of *Il6* in HeLa cells transiently expressing Regnase-1-WT or indicated mutants together with *Il6*. Cells were stimulated with IL-1 $\beta$  (10 ng/ml) for indicated time. (C) Immunoblot analysis of immunoprecipitates (IP: FLAG) and WCL from HeLa cells transiently expressing FLAG-Regnase-1-WT or indicated mutants. For the IL-1 $\beta$  stimulation, cells were stimulated with IL-1 $\beta$  (10 ng/ml) for 4 hours. L.C.: light chain. (D) Schematic illustration of Regnase-1 and the amino acid sequences of Regnase-1-WT, -ExoSx2, and ExoSAAx2. NTD: N-terminal domain, ZF: Zinc finger domain, CTD: C-terminal domain. (E) mRNA expression of *Il6* in HeLa cells transiently expressing Regnase-1-WT or indicated mutants together with *Il6*. (F) Secreted IL6 concentration in (E). (G) mRNA expression of *Il6* in HeLa cells transiently expressing Regnase-1-WT and IRAK1-WT or indicated mutants together with *Il6*. (H) The amount of *IL6* mRNAs immunoprecipitated with FLAG-Regnase-1-D141N or other indicated mutants in HeLa cells.

In (B), (E)-(H), bars represent mean values of biological replicates ( $n = 3$ ), and error bars represent standard deviation. *P*-values were calculated using unpaired, two-sided t-test. Data is representative of two independent experiments, each with three biological replicates.

**Figure 6**

14-3-3 inhibit nuclear-cytoplasmic shuttling of Regnase-1.

(A) Immunofluorescence analysis of HeLa cells transiently expressing FLAG-Regnase-1-WT treated with Leptomycin B (LMB) (10 ng/ml) for indicated time. (B)

The result of NES prediction of Regnase-1 by LocNES. Higher score indicates higher probability. (C) Schematic illustration of Regnase-1. The amino acid sequence shown in (D) is highlighted in blue. NTD: N-terminal domain, ZF: Zinc finger domain, CTD: C-terminal domain. (D) The amino acid sequences including S435/S439 and NES of Regnase-1 from mouse and other indicated vertebrates. (E) Immunofluorescence analysis of HeLa cells transiently expressing FLAG-Regnase-1-WT or indicated mutants. (F) Immunofluorescence analysis of HeLa cells transiently expressing FLAG-Regnase-1-WT or indicated mutants treated with LMB (10 ng/ml) for 1 hour. (G) Model of 14-3-3- and  $\beta$ TRCP-mediated regulation of Regnase-1. In the steady state, Regnase-1 shuttles between the nucleus and the cytoplasm and degrades target mRNAs such as *Irf6*. Under IL-1 $\beta$  or TLR-ligands stimulation, two different regulatory mechanisms suppress the activity of Regnase-1 not to disturb proper expression of inflammatory genes;  $\beta$ TRCP induces protein degradation of Regnase-1 and 14-3-3 inhibits nuclear-cytoplasmic shuttling and mRNA recognition of Regnase-1. In (A), (E), and (F), white scale bars indicate 20  $\mu$ m.

#### **Figure 1—figure supplement 1**

##### **Regnase-1 binds to 14-3-3 and $\beta$ TRCP in response to IL-1 $\beta$ stimulation**

Immunoblot analysis of immunoprecipitates (IP: Myc or IP: HA) and WCL from HeLa cells transiently expressing Myc-14-3-3 $\epsilon$  and HA- $\beta$ TRCP1 stimulated with IL-1 $\beta$  (10 ng/ml) for indicated time. The immunoprecipitates and corresponding WCL samples, both of which were used in Figure 1C, were applied to the same gel and the membranes were blotted with anti Regnase-1 antibody as well as anti-Actin antibody.

#### **Figure 1—figure supplement 2**

##### **Regnase-1 binds to 14-3-3 $\beta$ / $\gamma$ / $\epsilon$ / $\zeta$ / $\eta$ / $\theta$ but not 14-3-3 $\sigma$**

Immunoblot analysis of immunoprecipitates (IP: HA) and WCL from HeLa cells transiently

expressing HA-14-3-3 $\beta$ ,  $\gamma$ ,  $\epsilon$ ,  $\zeta$ ,  $\eta$ ,  $\theta$ , or  $\sigma$  stimulated with IL-1 $\beta$  (10 ng/ml) for 4 hours.

**Figure 2—figure supplement 1**

**Regnase-1 bands migrate slower in LPS-stimulated samples**

Immunoblot analysis of *Zc3h12a*<sup>WT/WT</sup> and *Zc3h12a*<sup>-/-</sup> thioglycollate-elicited PECs stimulated with LPS (100 ng/ml) for indicated time.

**Figure 2—figure supplement 2**

**Candidate spectra of Regnase-1 phosphopeptides with confident site localization.**

Only quantitatively altered phosphopeptides are shown. Fragment ions containing the N-(b-type ions) or C-(y-type ions) terminus are labeled with red (without neutral loss) or orange (with neutral-loss).

**Figure 2—figure supplement 3**

**Regnase-1-14-3-3 interaction is impaired in IRAK1/2 depleted cells**

HeLa cells were transfected with pX459 to knockout *IRAK1* and *IRAK2*. After the selection with puromycin, the cells were transfected with 14-3-3 $\epsilon$  and stimulated with IL-1 $\beta$  (10 ng/ml) for 4 hours. Immunoblot analysis of immunoprecipitates (IP: HA) and WCL is shown.

**Figure 2—figure supplement 4**

**Schematic illustration of IRAK1**

The result of secondary structure prediction is shown below. DD: Death domain, CSD: C-terminal structural domain.

**Figure 2—figure supplement 5**

**R663/K665A mutation does not abrogate IRAK1-mediated NF- $\kappa$ B activation**

Luciferase activity of HeLa cells transiently transfected with NF- $\kappa$ B luciferase reporter plasmid together with expression plasmids of IRAK1-WT or indicated mutants.

**Figure 2—figure supplement 6**

**IL-17A stimulation induces phosphorylation at S494 and S513 of Regnase-1**

Quantitation of phosphosites on Regnase-1 in HeLa cells stimulated with or without IL-17A (50 ng/ml) for 4 hours. Each dot shows phosphosite quantitative ratio between IL-17A+ and IL-17A-. Phosphosites with  $\log_2$  ratio  $> 1$  were colored with red. Black horizontal line shows Regnase-1 protein quantitative ratio derived from the average of non-phosphopeptide quantitative ratios, and its error bars show the standard deviation.

**Figure 2—figure supplement 7**

**Candidate spectra of Regnase-1 phosphopeptides with confident site localization**

Only quantitatively altered phosphopeptides are shown. Fragment ions containing the N-(b-type ions) or C-(y-type ions) terminus are labeled with red (without neutral loss) or orange (with neutral-loss).

**Figure 2—figure supplement 8**

**IL-17A stimulation induces Regnase-1-14-3-3 association**

Immunoblot analysis of immunoprecipitates (IP: HA) and WCL from HeLa cells transiently expressing HA-14-3-3 $\gamma$  and FLAG-Regnase-1-WT or indicated mutants stimulated with IL-17A (50 ng/ml) for 4 hours.

**Figure 4—figure supplement 1**

**Schematic illustration of *Zc3h12a* gene in mice**

The result of Sanger sequencing around S513 of Regnase-1 are shown below.

**Figure 4—figure supplement 2**

**The protein stability of Regnase-1-WT and S513A**

Immunoblot analysis of *Zc3h12a*<sup>WT/WT</sup> and *Zc3h12a*<sup>S513A/S513A</sup> thioglycollate-elicited PECs treated with LPS (100 ng/ml) and CHX (100  $\mu$ g/ml) for indicated time. CHX and LPS were

added at the same time.

**Figure 4—figure supplement 3**

***Il6* expression in *Zc3h12a*<sup>-/-</sup> PECs**

mRNA expression of *Il6* and *Zc3h12a* in *Zc3h12a*<sup>WT/WT</sup> and *Zc3h12a*<sup>-/-</sup> thioglycollate-elicited PECs stimulated with LPS (100 ng/ml) for indicated time.

Bars represent mean values of biological replicates ( $n = 3$ ), and error bars represent standard deviation.

**Figure 4—figure supplement 4**

**The stability of Regnase-1 target mRNAs**

The remaining mRNA levels of indicated genes in *Zc3h12a*<sup>WT/WT</sup> and *Zc3h12a*<sup>S513A/S513A</sup> MEFs. Actinomycin D (ActD, 10μg/ml) was added after 4-hour stimulation with IL-1β (10 ng/ml).

Dots represent mean values of biological replicates ( $n = 3$ ), and error bars represent standard deviation.

**Figure 4—figure supplement 5**

**S513A mutation of Regnase-1 does not affect gene expression**

Transcriptome analysis of *Zc3h12a*<sup>WT/WT</sup> and *Zc3h12a*<sup>S513A/S513A</sup> thioglycollate-elicited PECs stimulated with LPS (100 ng/ml) for indicated time. Several known Regnase-1 target transcripts are annotated. None of transcripts shows significant (adjusted p value < 0.05) difference between *Zc3h12a*<sup>WT/WT</sup> and *Zc3h12a*<sup>S513A/S513A</sup>.

**Figure 5—figure supplement 1**

**Regnase-1-ExoSx2-D141N binds to 14-3-3**

Immunoblot analysis of immunoprecipitates (IP: FLAG) and WCL from HeLa cells transiently expressing FLAG-Regnase-1-D141N or indicated mutants. L.C.: light chain.



**Figure 5—figure supplement 2**

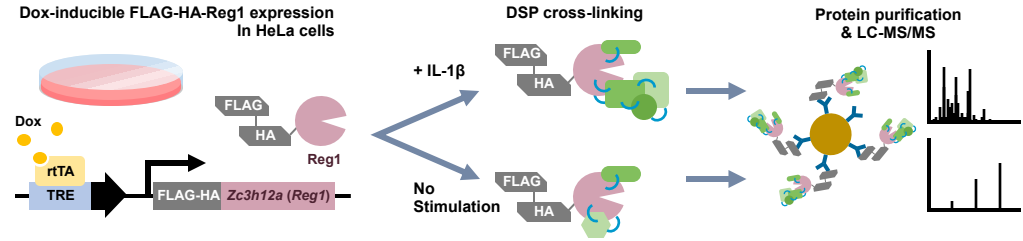
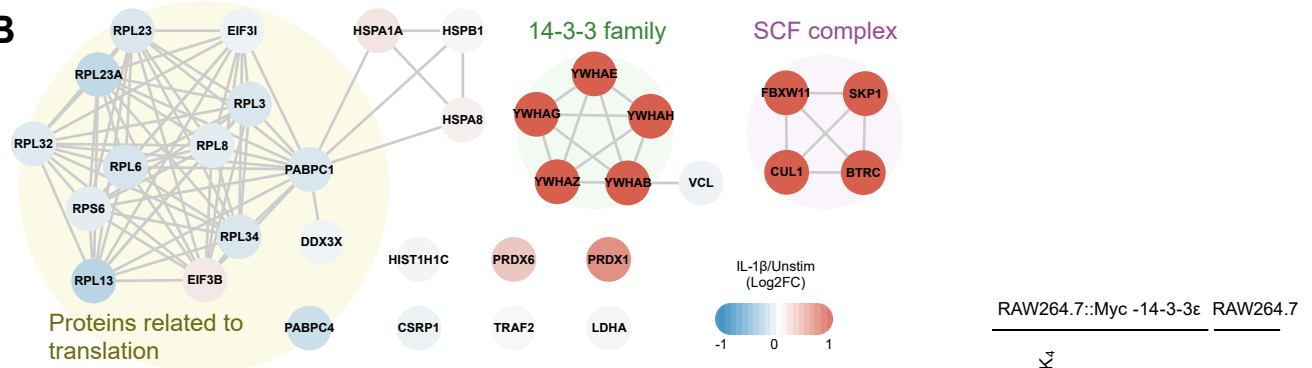
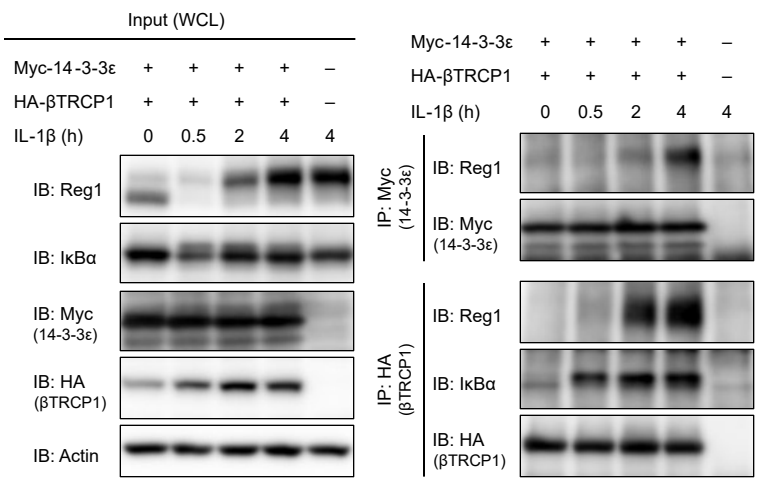
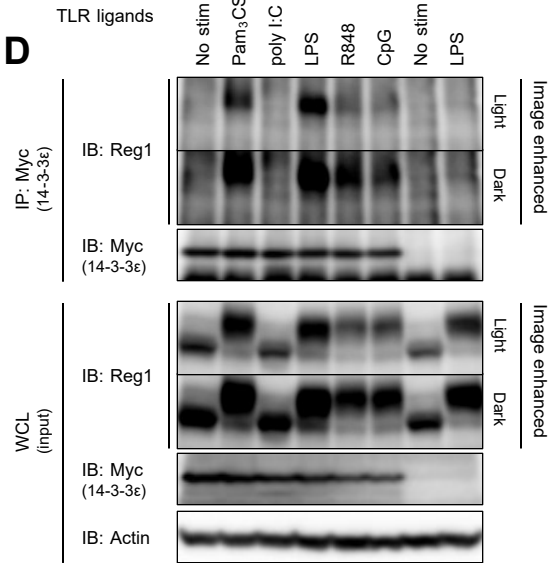
**Regnase-1-ExoSx2-D141N failed to bind to target mRNAs**

The amount of mRNAs immunoprecipitated with FLAG-Regnase-1-D141N or other indicated mutants in HeLa cells. The binding targets of Regnase-1 are denoted with \*.

Bars represent mean values of biological replicates (n=3), and error bars represent standard deviation. *P*-values were calculated using unpaired, two-sided t-test.

**Source Data Files**

Raw data of the results of immunoblotting are zipped in Source Data Files.

**A****B****C****D****Figure 1**

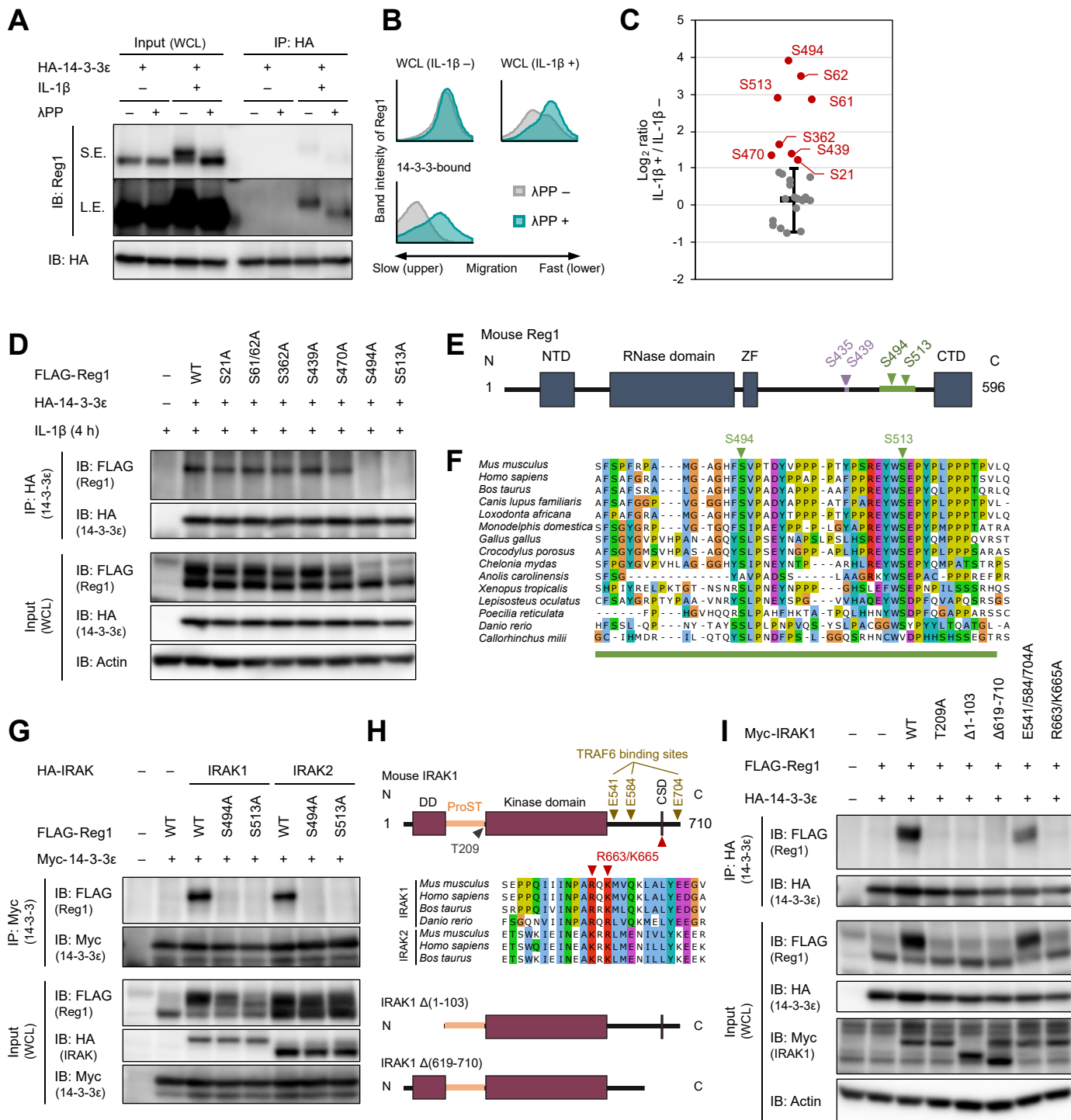


Figure 2

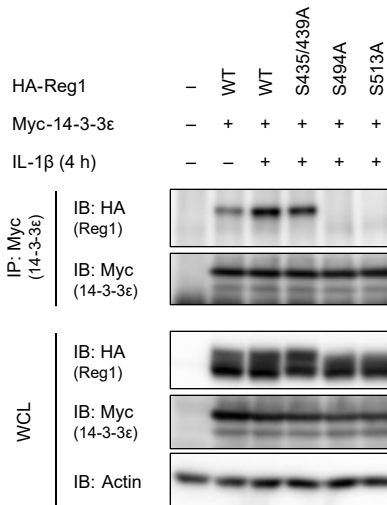
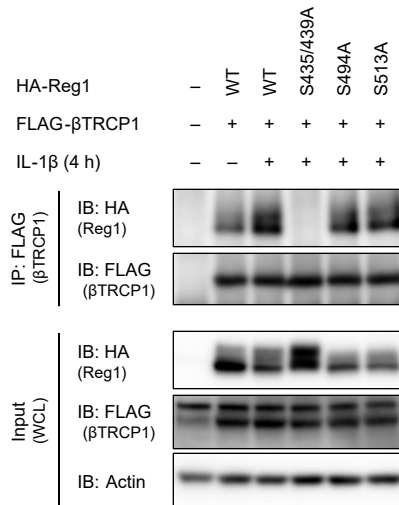
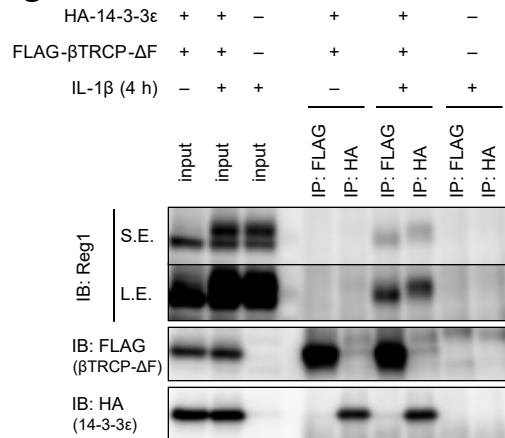
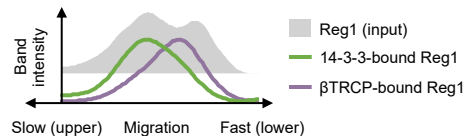
**A****B****C****D**

Figure 3

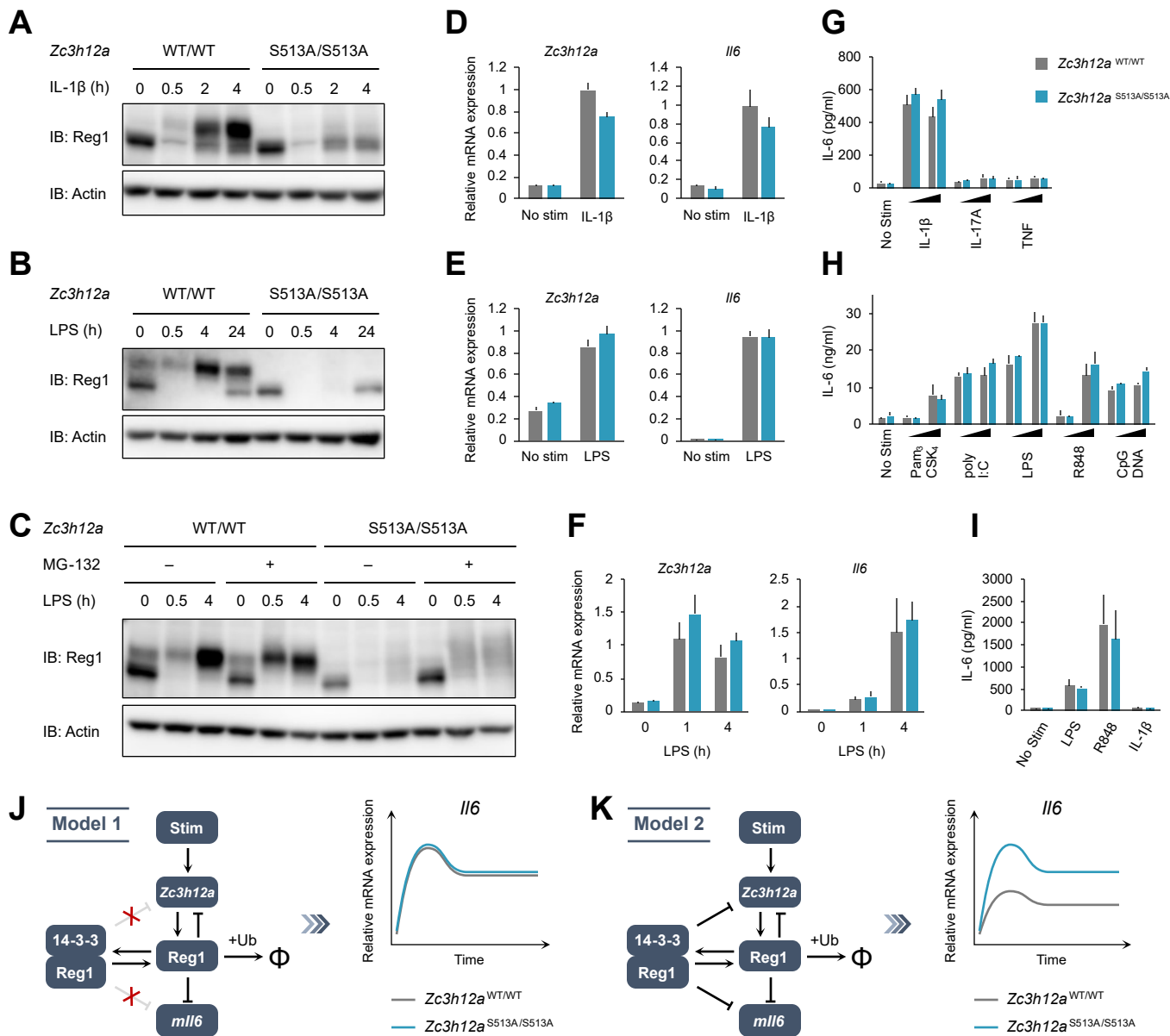


Figure 4

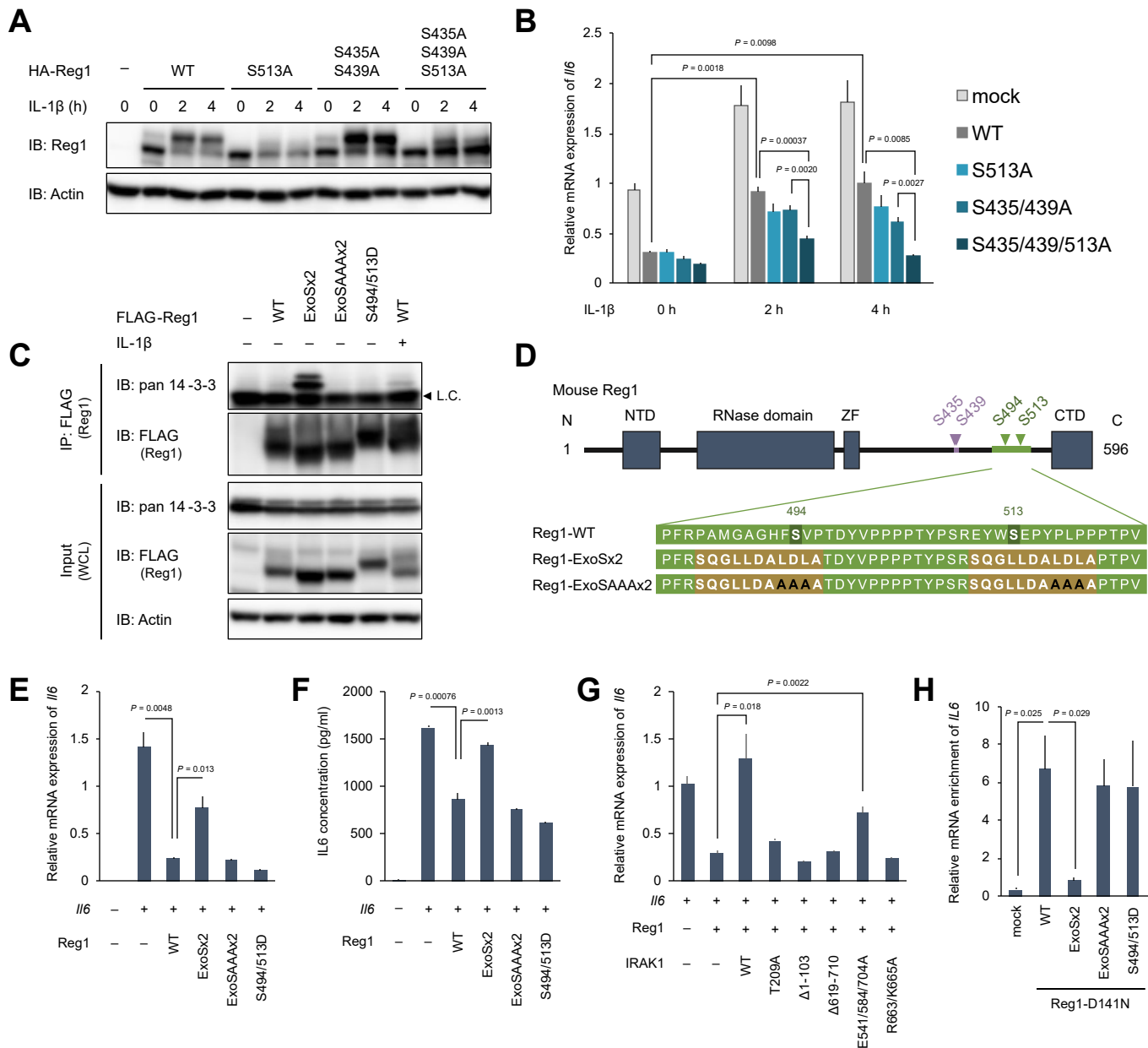


Figure 5

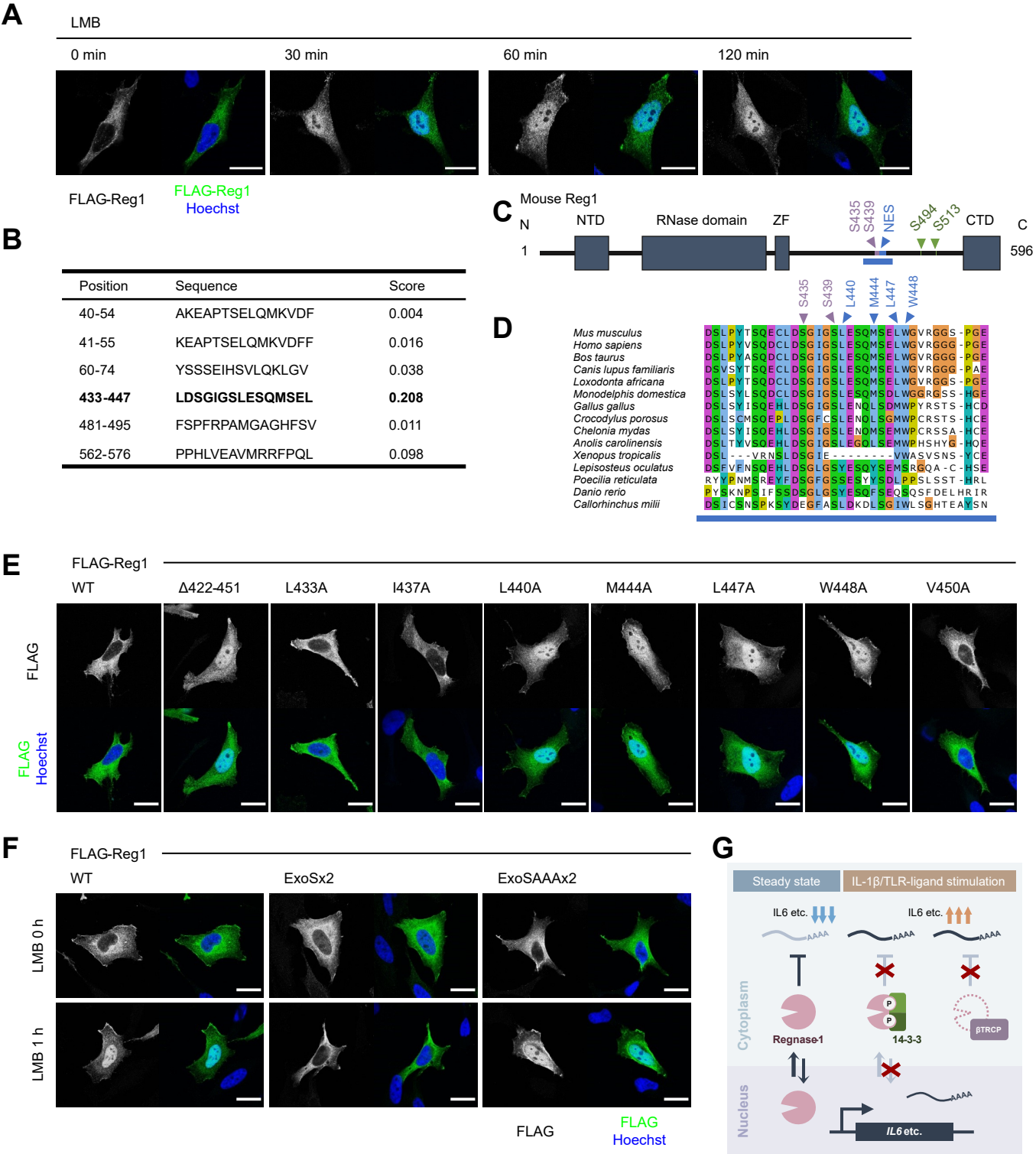


Figure 6

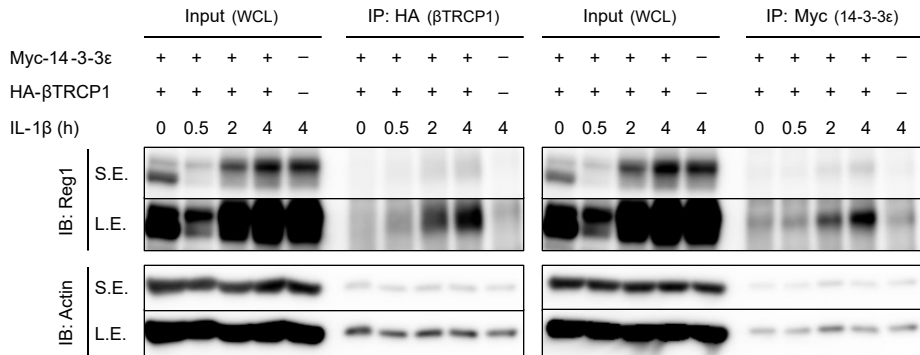


Figure 1-figure supplement 1



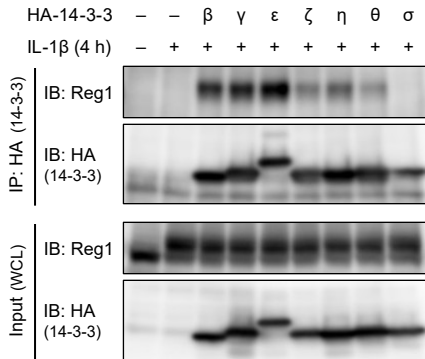


Figure 1-figure supplement 2

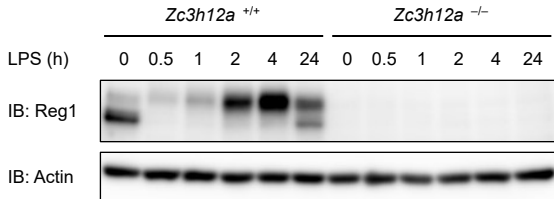


Figure 2-figure supplement 1

Mass spectrum of the protein GHSVPTDYPPTYPSPR. The x-axis is  $m/z$  (0-2000) and the y-axis is % of base peak (0-100). The base peak is at  $m/z$  999 (Y9). Other significant peaks are labeled with their amino acid sequence positions: b(2), b(3), b(4), b(5), b(10), b(11), b(12), b(13), b(14), b(15), b(16), b(17), b(18).

Mass spectrum of the protein KLVGYSSSEIH. The x-axis is  $m/z$  (400-1200) and the y-axis is % of base peak (0-100). The spectrum shows several peaks labeled with b and y fragment ions. A red arrow points to the y14 peak at  $m/z$  144. An inset shows the protein sequence KLVGYSSSEIH with the first 14 residues numbered 1-14.

[illegible]

Mass spectrum of the tryptic peptide ECLDSGILGSLQLMQMSLELMGVIR. The x-axis represents the mass-to-charge ratio ( $m/z$ ) from 0 to 1400, and the y-axis represents the relative intensity (% of base peak) from 0 to 100. The base peak is at  $m/z$  877. Other significant peaks are labeled with their b and y fragment ion designations: b(1), b\*(2), y(3), b\*(3), y(4), b(11)-98, y(5), b(6), y(6), b(9)-98, y(7), y(8), y(9), y(10), and y(11). The sequence ECLDSGILGSLQLMQMSLELMGVIR is shown at the top with fragmentation sites indicated by vertical lines and numbers 1 through 17.

Mass spectrum of the peptide A(G)Y(H)S(Y)G(S)K. The x-axis is  $m/z$  from 0 to 1000, and the y-axis is % of base peak from 0 to 100. The base peak is at  $m/z$  514. Other significant peaks are labeled with  $b$  and  $y$  ion series:  $y(6)$  at  $m/z$  98,  $y(6)+$  at  $m/z$  198,  $y(7)+$  at  $m/z$  298,  $y(4)$  at  $m/z$  398,  $y(5)+$  at  $m/z$  498,  $y(5)$  at  $m/z$  598,  $y(6)$  at  $m/z$  698,  $y(7)$  at  $m/z$  798,  $y(8)$  at  $m/z$  898, and  $y(6)$  at  $m/z$  998.

Mass spectrum of the LWSLEDR peptide. The x-axis represents the mass-to-charge ratio ( $m/z$ ) from 0 to 1000, and the y-axis represents the percentage of the base peak from 0 to 100. The base peak is at  $m/z$  598. Other significant peaks are labeled:  $y(1)$  at 174,  $b(2)$  at 216,  $b(3)$  at 258,  $y(3)$  at 274,  $y(4)$  at 316,  $y(5)$  at 358,  $y(6)$  at 398,  $y(6)-98$  at 500,  $y(5)-98$  at 598,  $y(6)-98$  at 698,  $y(6)$  at 798, and  $y(6)$  at 898. A chemical structure of the peptide LWSLEDR is shown at the top.

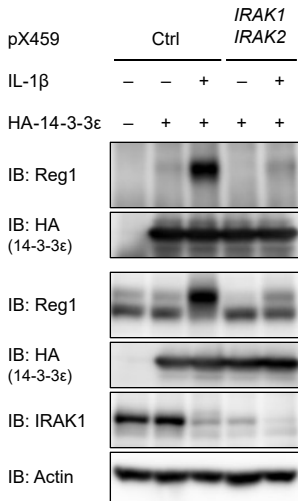


Figure 2-figure supplement 3

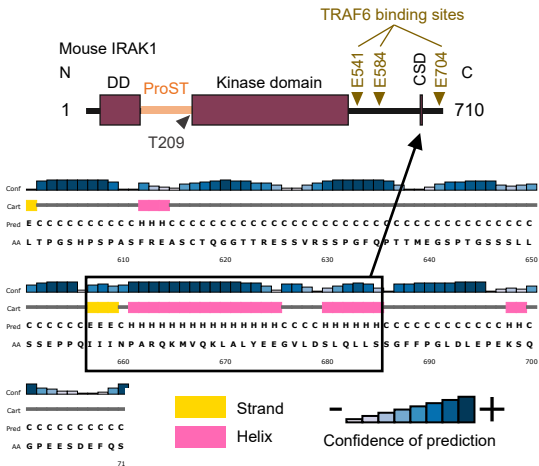


Figure 2-figure supplement 4

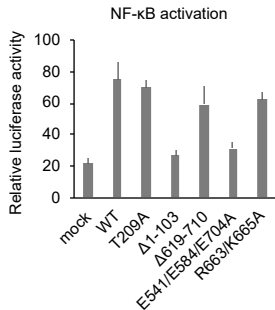


Figure 2-figure supplement 5

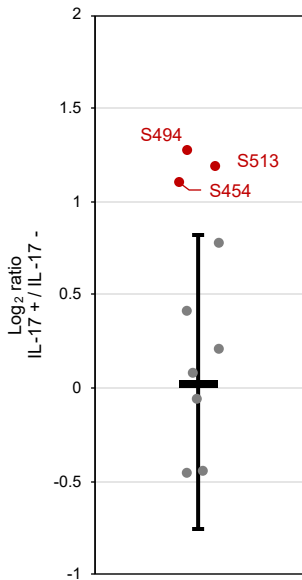
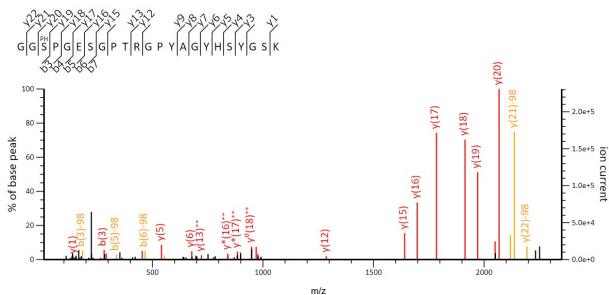
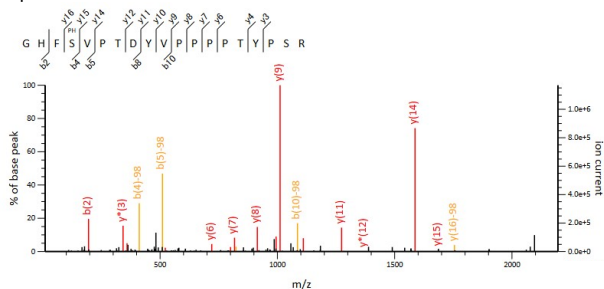


Figure 2-figure supplement 6

# Phosphosite: S454, Mascot ion score : 118



# pSite: S494 Mascot ion score: 67



# pSite S513 Mascot ion score : 31

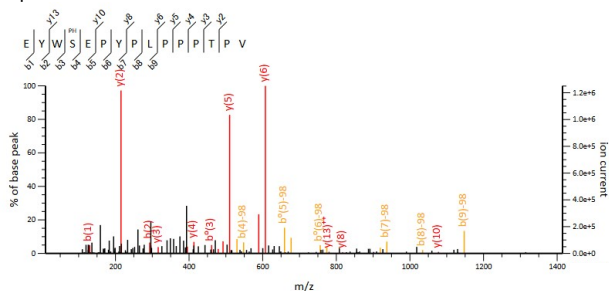


Figure 2-figure supplement 7



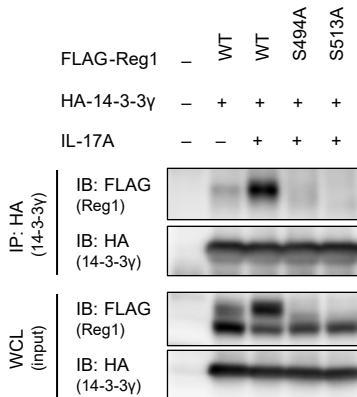
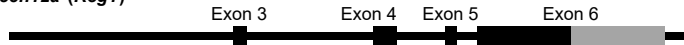
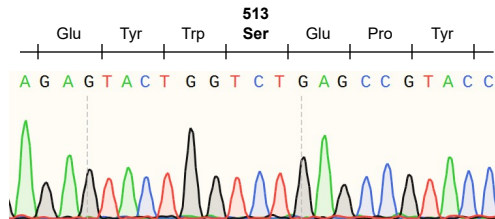


Figure 2-figure supplement 8

***Zc3h12a* (Reg1)**



***Zc3h12a1*<sup>WT/WT</sup>**



***Zc3h12a*<sup>S513A/S513A</sup>**

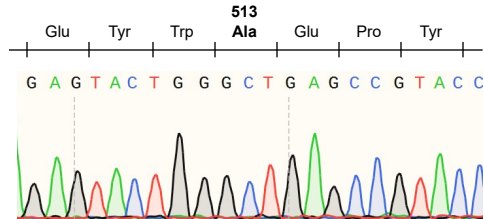


Figure 4-figure supplement 1

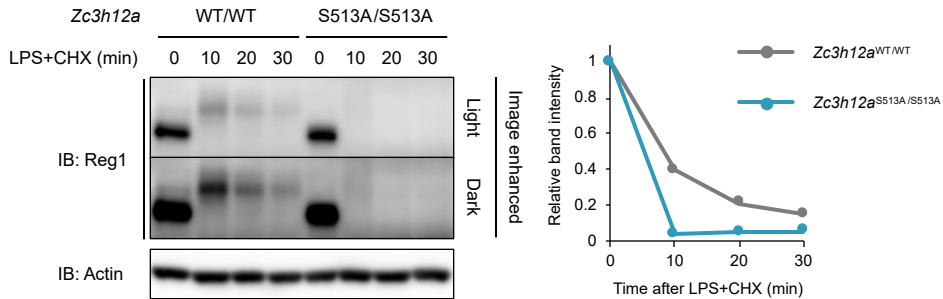


Figure 4-figure supplement 2

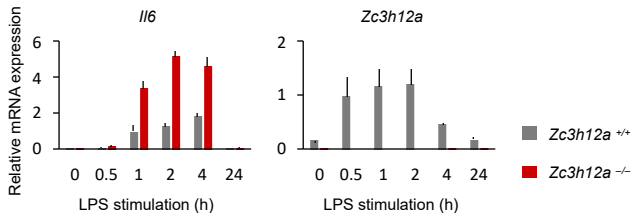


Figure 4-figure supplement 3

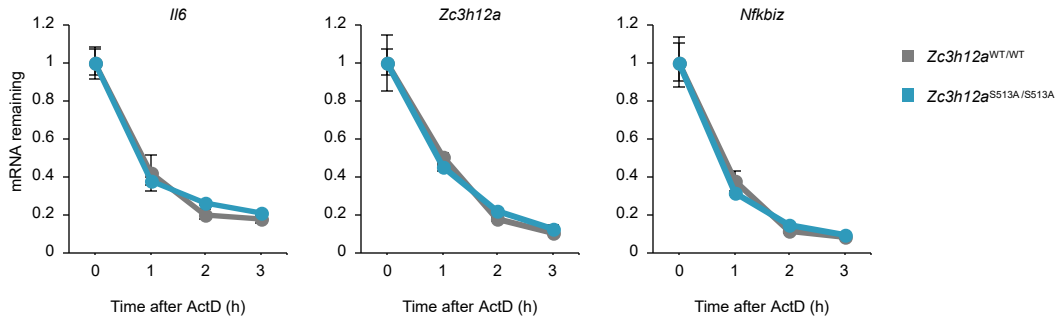


Figure 4-figure supplement 4

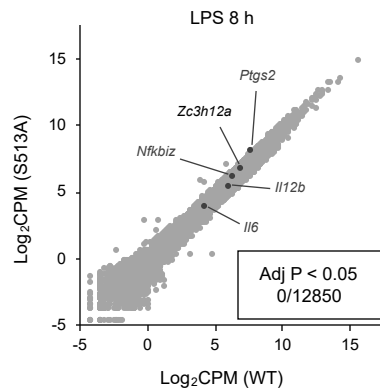
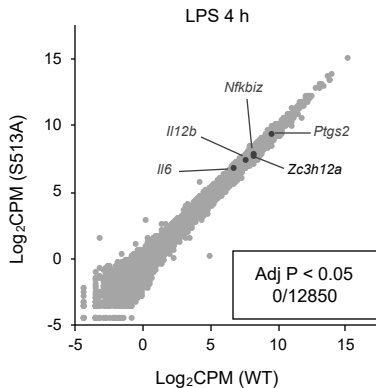
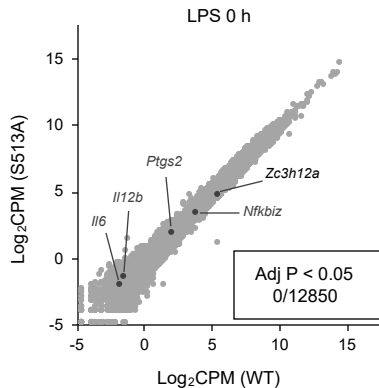


Figure 4-figure supplement 5

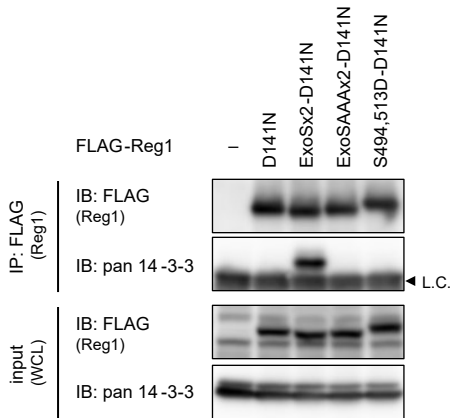


Figure 5-figure supplement 1

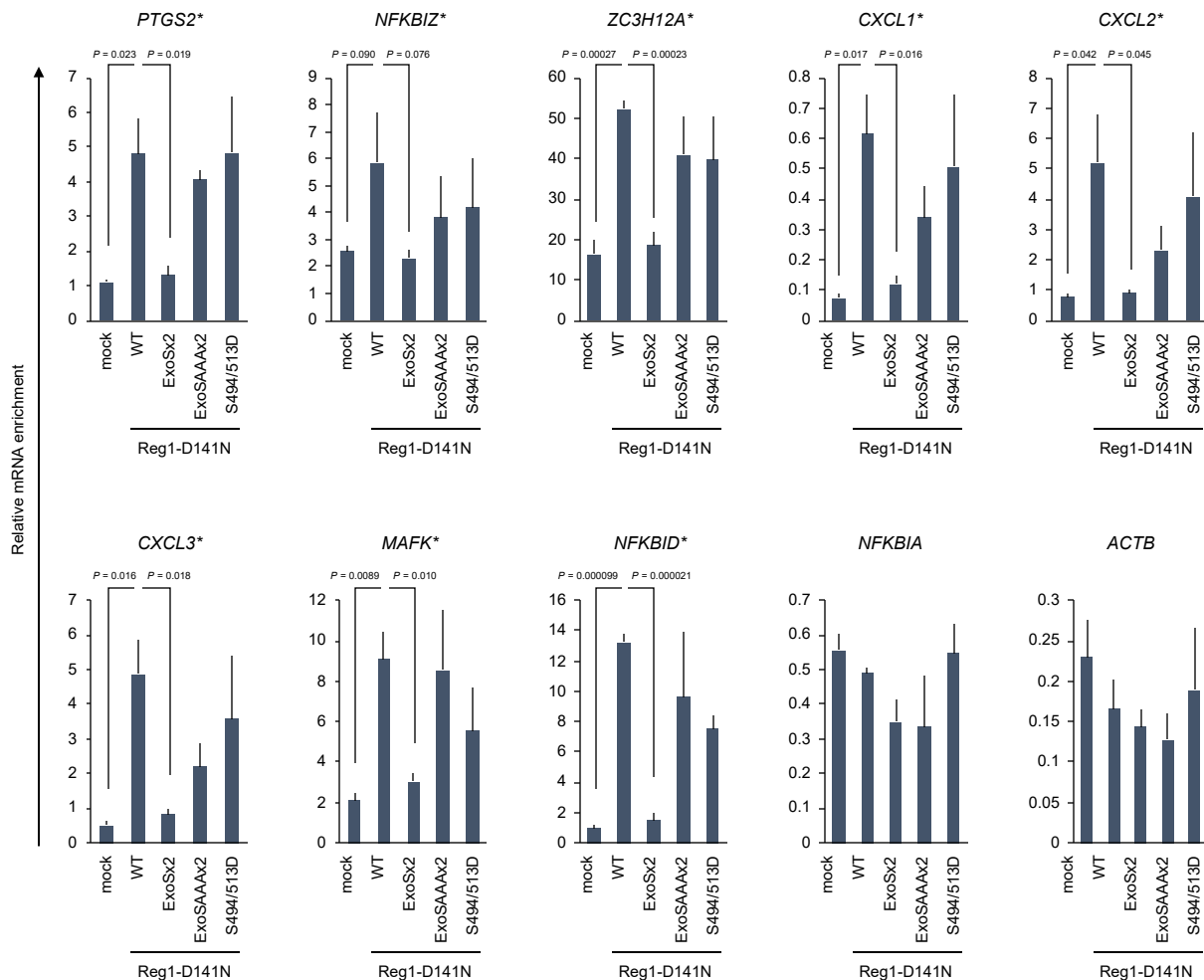


Figure 5-figure supplement 2